Journal of Medicinal Chemistry

Article

Binding and Proton Blockage by Amantadine Variants of the Influenza M2WT and M2S31N Explained

Christina Tzitzoglaki, Anna K. Wright, Kathrin-Maria Freudenberger, Anja Hoffmann, Ian Tietjen, Ioannis Stylianakis, Felix Kolarov, David Fedida, Michaela Schmidtke, Guenter Gauglitz, Timothy A. Cross, and Antonios Kolocouris

J. Med. Chem., **Just Accepted Manuscript** • DOI: 10.1021/acs.jmedchem.6b01115 • Publication Date (Web): 20 Jan 2017

Binding and Proton Blockage by Amantadine Variants of the Influenza $M2_{WT}$ and $M2_{S31N}$ Explained

Christina Tzitzoglaki,[1] Anna Wright,[2] Kathrin Freudenberger,[3] Anja Hoffmann,[4] Ian Tietjen,[5] Ioannis Stylianakis,[1] Felix Kolarov,[3] David Fedida,[5] Michaela Schmidtke,[4] Günter Gauglitz,[3] Timothy A. Cross,[2,6] Antonios Kolocouris[1,*]

[1] Section of Pharmaceutical Chemistry, Department of Pharmacy, National and Kapodistrian University of Athens, Athens, Greece.

[2] Institute of Molecular Biophysics and National High Magnetic Field Laboratory, Florida State University, Tallahassee, FL 32306.

[3] Institut für Physikalische und Theoretische Chemie, Eberhard-Karls Universität, Auf der Morgenstelle 18, D-72076 Tübingen, Germany.

[4] Jena University Hospital, Department of Virology and Antiviral Therapy, Hans Knoell Str. 2, D-07745 Jena, Germany.

[5] Department of Anesthesiology, Pharmacology and Therapeutics, University of British Columbia, Vancouver, British Columbia, V6T 1Z3, Canada.

[6] Department of Chemistry and Biochemistry, Florida State University, Tallahassee, FL 32306

20/01/2017~~18/01/2017~~

ABSTRACT

While aminoadamantanes are well-established inhibitors of the influenza A M2 proton channel, the mechanisms by which they are rendered ineffective against $M2_{S31N}$ are unclear. Solid state NMR, isothermal titration calorimetry, electrophysiology, anti-viral assays and molecular dynamics simulations suggest stronger binding interactions for aminoadamantanes to $M2_{WT}$ compared to negligible or weak binding to $M2_{S31N}$. This is due to reshaping of the M2pore when N31 is present, which in contrast to wild type (WT), leads: A) to the loss of the V27 pocket for the adamantyl cage and to a predominant orientation of the ligand's ammonium group toward the N-terminus and, B) to the lack of a helical kink upon ligand binding. The kink, which reduces the tilt of the C-terminal helical domain relative to the bilayer normal includes the W41 primary gate for proton conductance and may prevent the gate from opening, representing an alternative view for how these drugs prevent proton conductance.

INTRODUCTION

A proven vulnerability of influenza A infections is the blockage of the viral M2 proton channel. M2 is required for acidification of the virion interior during infection and neutralization of the trans-Golgi network during viral egress.[1] Amantadine ((*Amt*), **1**) (Scheme 1) is an established inhibitor of the influenza A/M2-mediated proton currents[2] and a licensed influenza A infection therapy.[3] The primary binding site of **1** is located within the pore of the tetrameric M2 transmembrane (M2TM) domain that forms the transmembrane proton transit path.[4,5] However, since 2005,[6] the **1**-insensitive Ser-to-Asn mutation at position 31 in M2 (S31N) has become globally prevalent,[7] abrogating the clinical usefulness of **1**[8] and possibly other previously reported M2 inhibitors.[9] Thus, new agents are needed to combat drug-resistant forms of influenza.

Based on the experimental solid state NMR (ssNMR) structure of the complex M2TM-**1**[4a,5a,b], the replacement of S31 residues at the drug binding site with the more polar and bulky Asn sidechains may induce the adamantyl ring to move deeper into the M2 pore, toward the C-terminus close to G34, where the pore of the helical bundle has its largest diameter, and drugs larger than **1** might be effective. We and others have searched for such larger drugs and found, for example compounds **5-7**, which are active against A/Calif/07/2009 (H1N1) virus encoding S31N but not against WSN/33 also bearing the same mutation.[10] However, while a preliminary ssNMR experiment of the S31N M2TM domain complexed with compound **5** showed evidence of drug binding, electrophysiology (EP) studies showed no blockage for the full length S31N M2 protein.[10a] These studies therefore indicate that more detailed experimental investigation and modelling are needed to explain the mechanisms by which aminoadamantanes are rendered ineffective against $M2_{S31N}$ in order to design effective drugs.

Recent molecular dynamics (MD) simulations showed that the ammonium group of **1** has a prevalent orientation toward the C-terminus of $M2TM_{WT}$ (Udorn), with the adamantane hydrocarbon cage shifted slightly toward N-terminus of the A30/S31 Cα sites[11-18], producing a

region of the pore devoid of water[17,18] consistent with blockage of proton transport and in agreement with ssNMR findings.[5c,20,21] In contrast, MD simulations of **1** in $M2TM_{S31N}$ from Gleed et al.[17b] and rimantadine in $M2TM_{S31N}$ from Alhadeff et al.[16] suggested that these compounds have a variable orientation, but with a propensity to have the ammonium group toward the N-terminus[17b,22] of the $M2TM_{S31N}$ pore (Figure 1). In this orientation water occupancy is not widely occluded in any configuration.[17] These studies[16,17b] presented a description of the Potential of Mean Force (PMF) curves of amantadine and rimantadine in interaction with the $M2TM_{S31N}$ pore but the main structural/interaction changes due to S31N and leading to aminoadamantane resistance were not defined. In addition, no experimental evidence is presented to date for the binding of aminoadamantane ligands in $M2TM_{S31N}$ pore. Nevertheless, the propensity of **1**'s amino group to orient towards the N-terminus was used for the successful design of **1**-polar head conjugates that were shown to be potent inhibitors of WSN/33 virus and proton conductance by $M2_{S31N}$[23]. A ssNMR analysis of a system including one of these compounds, a phenylisoxazole derivative linked with amantadine through a methylene bridge, with M2TM in membrane bilayers was realized. The results showed that the compound's heterocyclic ring system may be trapped by the V27 side chains at N-terminus of the M2TM-pore[24] with the isoxazole group forming hydrogen bonds with the N31 amide side chains.

We are interested to investigate how subtle changes in amantadine structure are related with the binding affinity against M2TM variants**.** We previously used molecular mechanics Poisson-Boltzmann surface area (MM/PBSA) to interpret thermodynamic profiles measured using isothermal titration calorimetry (ITC) for aminoadamantanes binding to the avian $M2TM_{Weybridge}$ ($M2TM_{Weybridge}$ has different two amino acids that do not line into the pore, i.e., V28→I28 and L38→F38 compared to $M2TM_{WT}$) in order to successfully prioritize aminoadamantane derivatives.[25] We also applied rigorous free energy binding calculations by the Bennett acceptance ratio **(**BAR**)** approach to accurately predict relative binding affinities of aminoadamantane

derivatives towards $M2TM_{WT}$ or $M2TM_{Weybridge}$ measured by ITC or other methods respectively.[26,27]

Here we investigate the interaction of aminoadamantane derivatives (Scheme 1) with $M2TM_{WT}$ and $M2TM_{S31N}$ both experimentally and by MD simulations, with the aim of determining how the S31N mutation leads to the inability of **1** and other aminoadamantanes to block S31N M2 proton transport. First, we measured binding constants of selected aminoadamantane derivatives with ITC against $M2TM_{WT}$ and $M2TM_{S31N}$ in dodecylphosphocholine (DPC) micelles at alkaline pH. Second, we applied a series of MD simulations (80 ns trajectories) of the $M2TM_{WT}$ and $M2TM_{S31N}$ complexes with **1-10** (Scheme 1) to analyze in some detail how the polar N31 amide side chains affect binding of an aminoadamantane ligand inside the M2TM pore. To this end, we suggest that repulsive forces between N31 and the adamantane ring may influence the orientation and binding interactions of the ligand, the overall stability of the complexes, and the shape of M2TM. Third, we performed Oriented Sample (OS) and Magic Angle Spinning (MAS) ssNMR experiments[28-30] on representative M2TM-ligand complexes at alkaline pH using both $M2TM_{WT}$ and $M2TM_{S31N}$ sequences to characterize the structural influence of compounds on the channel. Fourth, we selected and tested new synthetic derivatives with slightly larger or similarly-sized adducts, like **8** and **10**, than previously synthesized compounds **5-7**, **9** for their abilities to bind $M2TM_{S31N}$. We realized EP experiments for selected compounds against both WT and S31N M2 proteins to test M2 channel blockage and additionally measured the antiviral potency of the compounds against the naturally amantadine-resistant H1N1 influenza strain A/WSN/1933 (WSN/33 with $M2_{N31}$) and its reverse genetics-generated amantadine-sensitive variant with the amino acid substitution N31S in M2 (WSN/33-M2-N31S) using cytopathic effect inhibition (CPE) assays.

RESULTS

Binding affinities of aminoadamantanes to M2TM by ITC

ITC measurements[31] were determined for both $M2TM_{WT}$ and $M2TM_{S31N}$ tetramers at pH 8 corresponding to the closed state of the M2TM pore[32] (Table 1). Binding data for compounds **1**, **5**, **6-8** to $M2TM_{WT}$ measured in our previous work[26] were included in Table 1. Thus, as has been published recently[26] (see Tables 1 and S1) compounds **1-8** bind $M2TM_{WT}$. Compound **9** and the newly synthesized analogue **10**, which has a cyclohexane ring instead of the cyclopentane in **9**, bind $M2TM_{WT}$ with at least an order of magnitude lower dissociation constant (K_d) than those for **1-8**, possibly because their size do not enable them to fit well inside $M2TM_{WT}$. We note that techniques for measuring affinity against M2TM such as ITC correspond to models of molecular recognition for ligand binding to M2TM and do not necessarily reflect functional inhibition of M2 proton currents or in vitro inhibition of influenza A virus. For example, **9** inhibits $M2_{WT}$-dependent currents as measured by electrophysiology with an IC_{50} of 10 ± 2 μM (Table 4) and inhibited influenza A virus replication in infected cells with an IC_{50} of 3.92 ± 2.22 μM (Table 5) while compound **10** was inactive. Nevertheless, ITC and related techniques like Surface Plasmon Resonance (SPR) and structural techniques like ssNMR can provide useful insights for M2TM binding and trends in structure-activity relationships for the M2-aminoadamantane system. For example, compounds **1-4** did not bind efficiently to $M2TM_{S31N}$ according to ITC and previous SPR measurements for **1**[33] while **5**, **6** with larger adducts connected to adamantane bind weakly to $M2TM_{S31N}$ compared to $M2TM_{WT}$ according to ITC (Table 1) and ssNMR. The K_d values of low affinity binders (e.g. **5**, **6**, **9**, **10)** against $M2TM_{S31N}$, and **9** against $M2TM_{WT}$, possess relatively large errors due to the limitations of the ITC method (as explained in the Supporting Information). Subsequently comparison of the relative K_d values of compounds **5**, **6**, **9**, **10** do not reflect relative

binding affinity strength against $M2TM_{S31N}$. Nevertheless, although the quantitation of the ITC results against $M2TM_{S31N}$ is limited for this method, the measurements suggest that the K_d values of **5** and **6** against $M2TM_{S31N}$ are much smaller compared to $M2TM_{WT}$ suggest weaker binding to $M2TM_{S31N}$ (Table 1). Narrower linewidths and larger chemical shifts changes for **5** bound to $M2TM_{WT}$ compared to $M2TM_{S31N}$ were observed in the ssNMR spectra described below suggesting a reduction in dynamics for binding to $M2TM_{WT}$ and a more specific binding site, which in turn causes a significant reduction in hydration due to drug induced desolvation of the binding pocket.[31]

Solid state NMR of M2TM - aminoadamantanes complexes

OS ssNMR spectra

Drug binding to the channel pore of $M2TM_{WT}$ and $M2TM_{S31N}$ was evaluated using OS ssNMR experiments. Spectral correlation observed in these data sets, between anisotropic ^{15}N chemical shifts and ^{1}H-^{15}N dipolar coupling values for selectively ^{15}N-labeled backbone amide sites, gives rise to resonance patterns known as PISA (polarity index slant angle) wheels.[34,35] The shape, size and position of the PISA wheel for α-helical membrane proteins in uniformly oriented lipid bilayer preparations is determined by the helical tilt relative to the bilayer normal, and is sensitive to drug-induced structural perturbations. Previous investigations by Cross and co-workers have reported dramatic changes in anisotropic chemical shifts and dipolar coupling values for $M2TM_{WT}$ in the presence of **1**.[36] PISA wheel analysis of $M2TM_{WT}$ spectra in the *apo* state and in the presence of **1**[36] or **5** correlates the shifts with a substantial reduction in the tilt angle for the C-terminal region of the $M2TM_{WT}$ helix, following ligand binding. In contrast, $M2TM_{S31N}$ in the presence of **5** results in a uniform 5 ± 2° decrease in the helical tilt imparting a change to the entire helix-helix interface.[10a]

Here, to monitor changes in the resonance frequencies and to the resulting PISA wheel in the presence of other variants of **1**, a ^{15}N-V28,A30,I42 (VAI-M2TM) labeling scheme was used.

Residues 28 and 30 are in the N-terminal domain of the M2TM helix and I42 in the C-terminal region, and hence the labels effectively sample both segments. Resonance frequencies for these sites are well resolved allowing for a PISA wheel analysis of drug binding in the channel pore that induces small structural perturbations. The signals of these three pertinent and isotopically labeled backbone amides were shifted in nearly an identical fashion when **1** or **5** bind to the $M2TM_{WT}$ (Figure 2). As before, changes suggest only a slight perturbation to the N-terminus and a much more significant structural perturbation to the C-terminus with a change in the tilt angle from 32° to just 22°, while the N-terminal tilt changes by only a degree or two (Table 2).[4b,36] These results imply similar drug induced structural perturbations to the TM configuration of WT M2 protein in the presence of **1** or **5**.

For the binding studies to $M2TM_{S31N}$, no observable effect was detected for binding of **1**, while **5** induces smaller changes compared to those induced by the binding of **1** or **5** to $M2TM_{WT}$ based on the signals from the same three backbone amides (Figure 3). In addition, the linewidths are narrower when **5** is bound to $M2TM_{WT}$ compared to $M2TM_{S31N}$, suggesting less dynamics in the WT complex implying a tighter complex.

There is a small difference in the structure of $M2TM_{S31N}$ versus $M2TM_{WT}$ without drugs in lipid bilayers (black resonances in Figure 2 versus Figure 3). The $M2TM_{S31N}$ data suggests a helical tilt of approximately 38°, somewhat greater than the helical tilt observed in the WT structure (32°) consistent with prior characterizations.[4,36] While the binding of **1** to $M2TM_{WT}$ produced a 10° kink near G34 in each helix of the tetramer,[4b,36] binding of **1** produced no such structural change for the **1**-resistant $M2TM_{S31N}$. The shifts in the anisotropic resonance frequencies which resulted when **5** binds to $M2TM_{S31N}$ demonstrates a significant change in helical tilt from 38° to 33° in the tetrameric complex (Table 3). Based on these resonances that sample the N- and C- regions of the TM helix, the structural change appears to be a uniform change in tilt. Consequently, the residues facing the pore remain the same, but the interactions between helices that provide the tetrameric stability may change substantially. Upon binding of **1** or **5** to $M2TM_{WT}$ a kinked helix at G34 is

produced but when adding these compounds to $M2TM_{S31N}$ helices are not kinked at G34. Instead, when **5** binds to $M2TM_{S31N}$, the entire helix-helix interface changes with the ~5° reduction in tilt for each of the four helices.

The structurally similar aminoadamantanes **6-8** produced similar ssNMR results when added to $M2TM_{S31N}$ (Figure 4) in that the change in structure always reflected a uniform change in helical tilt. **8** is a new derivative, which was synthesized to test the effect of C-methylation to binding compared to N-methylation in **6**. The measured helical tilt angles are 28° for **6**, 31° for **7**, and 33° for **8**, with the latter compound yielding results that are similar to those induced by **5** (Table 3). For **5-8**, there is no evidence for partial binding, since the unbound states are not observed in the spectra with drugs present. With **5**, V28 appears to have multiple resonances (Figure 3) clustered on an anisotropic chemical shift of 160 ppm and a dipolar interaction of 4 kHz. The structural differences would be small, i.e. no more than 1° change in the orientation of the V27-V28 peptide plane with respect to the bilayer normal. This suggests that even with **5** on the timescale of 10-100μs there is no significant evidence for asymmetry in this tetrameric structure, i.e. there is no evidence from these three labeled sites that $M2TM_{S31N}$ bound with different compounds **1, 5-8** forms a dimer of dimer, as has been suggested for the S31N structure.[37,38] If such structures are present they must interconvert on a timescale faster than the difference in spectral frequencies in Hz. Furthermore, if this was occurring with significantly different structures there would be a reduction in the width and height of the PISA wheel, which was not observed. The intensity of the resonances varies, again especially for **5**, suggesting that the compound may have competing binding interactions with the pore leading to heterogeneity in the frequencies, the weakening of the A30 resonance and the small dispersion of the V28 resonances as described above. These dynamics are in sharp contrast to the intense resonance for I42 for $M2TM_{S31N}$ bound with **5**. The uniformity of the resonance intensities that result from the interaction with heterocyclic compounds **6-8** may suggest less dynamics and more potent binders than **5** to $M2TM_{S31N}$.

MAS spectra

To evaluate further the effect of **6** binding to $M2TM_{S31N}$, 2D N-Cα correlation magic angle spinning (MAS) ssNMR experiments were performed using uniformly ^{13}C,^{15}N-labeled V7, A30, S31 and G34 $M2TM_{S31N}$ (^{13}C,^{15}N-VANG labeled $M2TM_{S31N}$). The labeling used aims to explore the binding interactions of amantadine analogs into $M2TM_{S31N}$ pore through measuring the effect of binding to the chemical shifts of V27, A30, G34 and N31. In the $M2TM_{WT}$ the binding area includes the expanded area including V27, A30 and also G34, S31.[4a,5b] Spectra were obtained (Figure 5) for both the *apo* protein (blue) and for **6** bound (red) to the labeled $M2TM_{S31N}$. Addition of the drug to the $M2TM_{S31N}$ sample resulted in chemical shift changes for N31 and G34 of 1.2 and 2.1 ppm, respectively, V27 and A30 resonances remain unchanged, suggesting that they are not involved in binding, while the isotropic chemical shift perturbation of the N31 and G34 residues suggest the drug binding site for $M2TM_{S31N}$ suggesting either direct hydrogen bonding with the backbone or indirect hydrogen bonding through water molecules.[21] Significant ^{15}N and/or $^{13}C\alpha$ chemical shift changes at V27, S31, G34 have been reported when rimantadine is bound to $M2TM_{WT}$[20,21] with S31 experiencing a dramatic 7 ppm shift relative to the *apo* state.[21] Despite the observed chemical shift changes at residues N31 and G34 when **6** bound to the $M2TM_{S31N}$, cross peak intensity was not increased as was observed for the WT full length M2 in complex with rimantadine.[21] This suggests that the conformational heterogeneity of $M2TM_{S31N}$ was not increased for these residues in the presence of the drug. A reduction in dynamics which is in agreement with narrower linewidths would be anticipated with a specific binding site or a significant reduction in hydration due to drug induced desolvation of the binding pocket. The narrower linewidths and increased anisotropic chemical shifts for the $M2TM_{WT}$ and $M2TM_{S31N}$ bound to **5** (Figures 2, 3) illustrate reduced dynamics and weaker or less specific binding of the drug to the $M2TM_{S31N}$.

MD simulations of M2TM - aminoadamantanes complexes

Starting structure of protein ligand-complex

MD simulations of the complexes between **1**, 2-alkyl-2-aminoadamantanes **2-5** and cyclic derivatives **6-10** with both $M2TM_{WT}$ and $M2TM_{S31N}$ provide insights for the binding interactions and possible structural changes in the binding area. All of the ligands' amino groups were considered to be protonated according to model calculations preformed previously for ligands **1** and **6**.[25,26] The structure of the complex $M2TM_{WT}$-**1** (PDB ID 2KQT[4a,5b]) was used as a starting structure for the simulations of $M2TM_{WT}$-ligand complexes and of $M2TM_{S31N}$-ligand complexes. The PDB ID 2KQT[4a,5b] structure was chosen since it was determined at pH 7.5 and DMPC planar bilayers and vesicles[4a,5b], i.e., similar conditions to those used in our simulations. Subsequently only small structural changes are to be expected in M2TM structure during MD simulations of its complexes with ligands and the equilibration phase should be short. It has been shown that the stability of the binding region for **1** in the M2TM tetramer is increased considerably when using DMPC compared to other lipids.[39-42] In addition, 2KQT (ref. 5b) should be considered as the best structure of the amantadine bound state of M2TM since it utilized both isotropic chemical shift restraints and all of the orientational restraints of an earlier structure characterized by Cross and coworkers (see ref. 4a). The structure of the $M2TM_{S31N}$-ligand (**1-10**) complexes were generated from $M2TM_{WT}$-complexes by mutating S31 to N (see also Experimental Part).

Complexes of ligands with $M2TM_{WT}$

The MD simulations of the $M2TM_{WT}$-ligand complexes reached equilibration in less than 40 ns with the protein system having full flexibility. The RMSDs values (Table S2) were ≤ 1.6 Å for M2TM Cα-carbons with respect to the initial structure of the production period[4a,5b] suggesting that $M2TM_{WT}$-ligand (**1-8**) complexes were very stable and the M2TM tetramer structure was

considerably unchanged in the course of the simulation. The mean values of the N-terminal and the C-terminal helical tilt of $M2TM_{WT}$ for the complexes with **1, 5** from the corresponding MD trajectories were measured to be 31°, 18° and 31°, 19° respectively and are in very good agreement with the values of 32°, 22° and 32°, 22° determined by OS ssNMR (Table 2). As noted above the starting structure 2KQT[4a,5b] having helical domain tilt angles of 31°, 19° were determined in similar conditions to those used in our MD simulations by Cross and coworkers.[4a] Even so these findings suggest that the ligand-$M2TM_{WT}$ complex was successfully equilibrated and the conditions were well adjusted to produce consistent results. Consistent with the experimental findings[5b,c] and previous observations,[25,26] the ammonium group of the aminoadamantane compounds was oriented towards the C-terminus with angles of < 77° between the C-N bond of the ligand and the membrane's normal (Table S2). The complexes of compounds **1-8** inside the M2TM lumen are stabilized through: a) formation of hydrogen bonds between their ammonium group and water molecules in the region between H37 residues and the ligand and b) van der Waals interactions between adamantyl group and a lipophilic pocket formed by V27 and A30 side chains (see Figure 6). This binding area is in accordance (a) with the ^{15}N chemical shifts perturbations for V27, A30 and S31 in complexes between **1** or 3-azaspiro[5,5]undecane and $M2TM_{WT}$ compared to the *apo* $M2TM_{WT}$.[39] and, (b) with the measured distance of 4.5 Å between G34Ca and the methyl group of rimantadine from REDOR ssNMR experiments in studies of the full length protein.[21] In addition, for complexes of $M2TM_{WT}$ with **1-8**, the distance between the adamantyl ring of the ligand and the center of mass of the four V27 (V27-Ad) varies between 4 and 4.9 Å, and the distance between the adamantyl ring of the ligand and the center of mass of the four A30 (A30-Ad) varies between 0.5 and 1.4 Å (Table S2). The position of the adamantyl ring inside the lumen was similar for ligands **2-8** differing from **1** only by 0.2-0.6 Å. To account for the position of the ligands towards the C-end we measured the distance between the center of mass of the four V27 and the ammonium nitrogen of the ligand (V27-N^+) which varied between 7.1 and 7.8 Å (Table S2). According to the measures in Table S2 hydrogen bonding ability is higher for the subset of ligands **1-5, 9, 10** than for the

subset **6**, **8** or **7**. Thus **1-5, 9, 10** can form on average 3 hydrogen bonds with neighboring water molecules, **6**, **8** can form 2 hydrogen bonds, and **7** one hydrogen bond respectively (Table S2). This is what was expected since **1-5, 9, 10** have a primary ammonium group, **6**, **8** have a secondary ammonium group and **7** have a tertiary ammonium group. For ligands **3-8** which include a carbon substituent at C-2 adamantane position the molecule is rotated in order to avoid repulsive van der Waals forces of the alkyl group with the symmetric M2TM pore. The average angle between the pore axis and C-N bond vector was increased progressively according to the alkyl group size, i.e., from 13.5^{o} for **1** to 25-35° for **2-8** (Table S2). Although all ligands **1-8** have similar binding mode as shown from the OS ssNMR spectra of complexes including **1, 5** (Figure 2), a subtle compromise between hydrogen bonding and hydrophobic interactions with key pore residues, such as V27, A30, affects the ligand tilt inside the pore and its different binding strength as shown by the ITC results (Table 1, Table S1). The adamantyl ring is slightly toward the N-terminus compared to the A30/S31 Cα, producing a region without water molecules. Snapshots of the simulation complexes with **5**, **6** are shown in Figure 6.

The MD simulations suggest that the $M2TM_{WT}$-ligand complex stability is reduced when a sizeable adduct is attached to adamantane, i.e., the M2TM pore does not efficiently accommodate the large adducts in compounds **9** and **10**. This is in accordance with the weak or no binding respectively of these drugs according to the ITC results (Table 1). For example, the MD simulations showed that the stability of the complex is considerably reduced in the case of **10** where after 80 ns the ligand is shifted toward the N-terminus; the mean distances of the trajectory V27-Ad, A30-Ad and V27-N^{+} are 3.5 Å, 4.7 Å and 2.1 Å, respectively, suggesting a loosening of the M2TM-complex integrity at the N-terminus (a snapshot of the simulation complex with **10** is depicted in Figure S1.a).

Complexes of ligands with $M2TM_{S31N}$

In the starting configuration of $M2TM_{S31N}$-aminoadamantane ligand complex the ammonium group points toward the C-terminus forming H-bonds with waters between the ligand and H37 residues as in the $M2TM_{WT}$ pore. The MD simulations of the complexes between $M2TM_{S31N}$ and **1-8** reach equilibration in less than 60 ns with the protein system having full flexibility. In complexes with $M2TM_{S31N}$ the ligand is more mobile inside the pore having a propensity to orient its ammonium group toward the N-terminus, in contrast to $M2TM_{WT}$-ligand complexes where the ligand forms a strong complex with ammonium group oriented toward the C-terminus. Thus, after a few ns of unrestrained dynamics the ligand moves toward the C-terminus by ~2 Å, probably because the adamantyl group is repelled by the polar N31 side chains resulting in the loss of the V27 lipophilic pocket, and the molecule rotates 180º through an attraction to the polar environment around N31. This finding is consistent with the narrower linewidths and larger chemical shifts changes for $M2TM_{WT}$ when bound with compound **5** compared to $M2TM_{S31N}$ as observed in the ssNMR spectra suggesting a stronger binding interaction with $M2TM_{WT}$. In addition waters are transferred from the region between the ligand and H37 to the area around N31 where the drug's amine can interact with the carbonyls of the N31 amide groups and waters around the amide side chains. Snapshots of the MD simulation complexes of $M2TM_{S31N}$ with **1**, **5**, **6** and **10** are depicted in Figure 7. The MD runs showed that by progressively increasing the size of the adduct connected to the adamantyl moiety in complexes with **2-8** the ammonium group orientation turns toward the N-terminus, and the drug keeps this orientation during the entire simulation period. While this change was observed for **1** after ~ 20 ns of production, the time needed for the aminoadamantane ligand to rotate towards the N-terminus may be increased for some larger adducts. For example, in the case of **5** the ligand's ammonium group keeps its orientation toward the C-terminus during the first 40 ns and then the molecule turns towards the N-terminus until the end of the 80 ns production time. While no significant conformational change was observed for $M2TM_{31N}$ tetramer in its complexes with **1-8** during the production period, the RMSDs for $M2TM_{S31N}$ Cα-carbons were ≤ 2.8 Å from

the initial structure[4a,5b], i.e., 1 to 1.5 Å higher than the RMSDs for $M2TM_{WT}$ Cα-carbons suggesting less dynamics for $M2TM_{WT}$ complexes (Table S3). The mean values of the helical tilt angles for the complexes of **1**, **5-8** with $M2TM_{S31N}$ from the corresponding MD trajectories were measured to be ~ 34°, 31°, 28°, 33°, 31° respectively and are close to 38°, 33°, 28°, 31° and 33° determined by OS ssNMR (Table 3). The uniformly tilted helical structure is a conversion form the initial kinked state in the 80-ns MD, where the starting structure reflects a homology model of 2KQT.[4a,5b] Here the major finding is the lack of kinked helices in $M2TM_{S31N}$ compared to the OS ssNMR structure when **1** binds $M2TM_{WT}$ suggesting than the MD simulations describe well the ligand-$M2TM_{S31N}$ structure.

For most of the ligands **1-8** the mean angle between the C-N bond vector and the normal of the membrane is > 140° for more than 40 ns of the simulation reflecting the propensity of ammonium group to orient towards the N-terminus (Table S3). The distance between the center of mass of the four V27 and the adamantyl ring of the ligands **1-8** (V27-Ad) was longer than in complexes with the $M2TM_{WT}$, which is consistent with an orientation of the ammonium group towards the N-terminus. On average, the adamantyl ring in the $M2TM_{S31N}$ was found to be ~ 1-2 Å toward the C-terminus compared to the $M2TM_{WT}$ complexes. Accordingly, the distance between the center of mass of the four V27 and the ligand's amine nitrogen in $M2TM_{S31N}$ complexes was shorter by 3-3.5 Å compared to $M2TM_{WT}$ complexes. In addition especially for the ligands with large adducts the adamantyl ring is positioned toward the C-terminus close to G34 (see distances A30-Ad and G34-Ad in Table S3) whereas in the $M2TM_{WT}$ complexes, adamantyl ring is shifted toward the N-terminus embraced by V27 and A30. The sum of the H-bonds between the ammonium groups of the ligands and waters and between the ammonium groups and the N31 side chain amides was on average three hydrogen bonds for the primary ammonium groups (ligands **1-5**), two hydrogen bonds for secondary (ligands **6** and **8**) and one hydrogen bond for tertiary ones (ligand **7**) (Table S3). Compounds **9** and **10** form three hydrogen bonds only with water molecules in the vicinity of N31 close to the wall of the pore, possibly because the ammonium group is sterically

crowded between the adamantyl and cycloalkane rings and cannot reach the side chains carbonyls of N31 (Table S3). In compound **10**, due to the large hydrocarbon framework, the adamantyl ring moves more than in any other compound toward the C-terminus, i.e., the distance between the center of mass of the four V27 to the adamantyl cage was 3.7-2.3 Å longer than **1-8** to fit inside the pore close to G34 and the distance between the center of mass of the four G34 to the adamantyl cage was 2.7 Å. A snapshot of the simulation complex with ligand **10** is depicted in Figure 7.

Electrophysiology results of aminoadamantanes blockage using full-length M2

1, its isomer **2**, and three compounds with sizeable adducts (**5**, **6**, and **9**) were assessed for their ability to inhibit low pH-dependent proton currents induced by full-length M2 protein (A/California/07/2009 with $M2_{N31}$) in transiently-transfected, voltage clamped HEK cells (Table 4).[10a,43] Data for compounds **1**, **2**, **5** were reported previously.[10a] It was found that none of these compounds blocked inward proton currents better than **1**, either following a standard 3-minute exposure to compound or after prolonged exposure for 30 minutes. These EP-based results indicated that the compounds were unable to block the full-length M2 channel encoding N31. However, when this M2 protein was modified to encode the **1**-sensitive S31 sequence (through an N31S mutation), all compounds inhibited proton currents with IC_{50}s of 10 μM or less (Table 4); by increasing adduct size the blocking effect of inward proton currents is reduced.

In vitro testing of aminoadamantanes against influenza A virus

The antiviral potency of the compounds **1-10** was measured against WSN/33 (H1N1) bearing the M2 S31N mutation[44] and its amantadine-sensitive variant WSN/33-M2-N31S[26] in MDCK cells with

CPE inhibitory assay.[45,46] Compounds **1-9** showed sub-micromolar IC_{50} values against WSN/33-M2-N31S but were inactive against WSN/33 (Table 5). Compound **10** was inactive against both strains. The selectivity index (CC_{50}/IC_{50}) of compounds **4-7** was comparable to **1**. The inhibition efficiency showed stringent head-ammonium group requirements for inhibition of amantadine-sensitive influenza A viruses - a result consistent with ITC and EP results.

DISCUSSION

Unraveling the binding differences for aminoadamantanes to $M2TM_{S31N}$ and $M2TM_{WT}$

Based on the MD simulations results and experimental findings, the molecular basis for weak binding and the inability of aminoadamantanes to effectively block $M2_{S31N}$ is described. The results of the experimental data from ssNMR and ITC experiments directly correlate with the MD simulation results showing that aminoadamantane derivatives are weaker binders in the pore of $M2TM_{S31N}$ compared to $M2TM_{WT}$ and that **5-8** are stronger binders compared to **1-4** against $M2TM_{S31N}$.

The S31N mutation of M2TM results in a shift of the hydrophobic adamantyl ring toward the C-terminus thereby losing the stabilizing hydrophobic interactions of the V27 isopropyl groups with the adamantyl ring that is present in the $M2TM_{WT}$. The bulky N31 side chains are oriented toward the N-terminus and the V27 side chains and the ammonium group of the ligands is also turned toward the N-terminus to form significant hydrogen bonding interactions with the polar N31 side chains and surrounding waters. This ammonium group orientational preference of amantadine and rimantadine has been previously noted by Gleed et al.[17b] and Alhadeff et al.[16]. The hydrogen bonding interactions with N31 is consistent with the MAS experimental data performed with

compound **6** showing a chemical shift perturbation for N31 and G34 compared to the *apo* $M2TM_{S31N}$. Distance measurements from ssNMR experiments showed the preference for the ammonium group of the aminoadamantane drugs orienting toward the C-terminus in $M2TM_{WT}$[5c] and toward the N-terminus in a complex of $M2TM_{S31N}$ with a conjugate of **1** having a phenylisoxazole polar head.[24] In this class of conjugates[23b-d] additional van der Waals interactions with the N-terminus stabilizes the ligand resulting in potential anti-influenza drugs. Here, where the aminoadamantane ligands, such as **1-8**, are hydrogen-bonded with the polar N31 environment, favorable van der Waals and hydrophobic interactions as those in $M2TM_{WT}$ are missing. In the $M2TM_{WT}$ the adamantyl ring is well accommodated by the V27 and A30 side chains and sizeable adducts such as ligands **5-8** additionally fill the region between A30 and G34 (Figures 1 and 6) but in $M2TM_{S31N}$ the adamantyl ring is close to A30 and in the vicinity of G34 (see Tables S2, S3) lacking a favorable hydrophobic pocket. This is consistent with the absence of chemical shift perturbations for V27 in the NCA MAS spectrum of **6** bound to $M2TM_{S31N}$ in comparison with the *apo* $M2TM_{S31N}$ compared to the significant chemical shift changes at V27, S31, G34 which have been reported when rimantadine is bound to $M2TM_{WT}$ relative to the *apo* state.[20,21] These structural differences can be clearly observed in Figures 6 and 7. The lack of favorable van der Waals interactions results to less stable complexes and a weaker binding for aminoadamantane ligands consistent with the much smaller K_d values of **5** and **6** by ITC against $M2TM_{S31N}$ compared to $M2TM_{WT}$ (Table 1). In addition, linewidths are narrower for the $M2TM_{WT}$-complex with **5** compared to the $M2TM_{S31N}$ complex suggesting less dynamics consistent with stronger interactions for the aminoadamantane derivatives in complexes with $M2TM_{WT}$. The RMSDs for M2TM Cα-carbons are 1.0-1.5 Å higher for the trajectories of $M2TM_{S31N}$ compared to $M2TM_{WT}$ complexes further suggesting more dynamics and weaker interactions in the S31N complexes.

In **1** and analogs with small adducts the adamantyl ring has a only a limited hydrophobic contact with A30 and is close to polar N31 side chains which exert repulsive forces on adamantyl ring. It should be noted that trajectories sampled in the MD simulations of ligands in the pore were

of 80 ns length, i.e., they are much shorter than the microsecond to millsecond time scales sampled by ssNMR. The MD runs of the complexes of **1-4** with $M2TM_{S31N}$ showed qualitatively that these molecules can't bind $M2TM_{S31N}$ because significant favorable van der Waals interactions are missing. This can be observed from snapshot for complex of **1** with $M2TM_{S31N}$ in Figure 7. In molecules **5-8** with sizeable adducts of the adamantyl ring fill effectively the region between A30 and G34 and the interactions needed for binding are slightly improved resulting in weak binding to $M2TM_{S31N}$ as compared to no binding for **1-4**. This can be observed from snapshots for complexes of **5**, **6** with $M2TM_{S31N}$ in Figure 7. Indeed, **1** did not bind as documented by the OS ssNMR spectra (Figure 3), but larger adducts as those present in compounds **5-8** appear to stabilize weak binding of the drug in the region between A30 and G34 (see Figure 7) and this is in accordance with the results from OS ssNMR spectra for weak binding of compounds **5-8** (Figures 3, 4) to $M2TM_{S31N}$. In addition, we were not able to detect any binding for **1-4** with $M2TM_{S31N}$ using ITC while we obtained approximate binding constants for **5**,**6**,**9**,**10** (Table 1). NMR data were not obtained for **9** and **10** because they produced disordered lipid bilayers. Thus, the results from the combination of simulations and experiments showed that **1** (and similarly **2-4**) did not bind $M2TM_{S31N}$ contrary to the weak binding for **1** previously suggested from short simulations[17b] but **5-8** having sizeable adducts display weak binding.

While binding strength of aminoadamantanes against $M2TM_{WT}$ was sensitive to modification of the adduct, the $M2TM_{WT}$-aminoadamantane complex stability was found to be very sensitive to the adduct size, as shown by the ITC and MD simulation results when considering **9** and **10** that produces unstable complexes. The MD simulations clearly show that **10** moves considerably toward the N-terminus of the pore losing specific binding interactions. Ligands **9** and **10** cause a dramatic reduction in affinity for $M2TM_{WT}$ compared to **1-8** but did not affect $M2TM_{S31N}$ affinity, which seems to be similar with that of **5** and **6**. The forces that cause the rotation of the adamantyl ring in the M2 pore appear to be inherent in the shared amine group and are not greatly perturbed by the other ligand variations as characterized by MD and OS ssNMR for adducts **1-4**, **5-8** against

$M2TM_{S31N}$. Taken together, the results from the combination of MD simulations, ITC and OS ssNMR showed no binding for **1** and similar in size analogues and only weak binding for sizeable adducts. The binding is more specific as showed by the more stringent head-ammonium group requirements in the binding pocket of $M2TM_{WT}$ than in the $M2TM_{S31N}$ according to the ITC but also as showed by the EP experiments and anti-viral assay results.

Thus, EP experiments indicate that the aminoadamantanes block the S31 but not the N31 full-length M2 protein. Notably, while the secondary gate formed by the V27 residues in the $M2TM_{WT}$[11] has the potential to limit water access to the pore the hydrophilic asparagine sidechains make this environment less hydrophobic and diminish the effectiveness of the V27 gate in the $M2TM_{S31N}$ pore. In the mutant waters are observed above and below the ligand and in a few snapshots between the ligand and the wall of the pore suggesting a relatively free passage through the $M2TM_{S31N}$ lumen despite the presence of the ligand.[12,17,18] (snapshots from the simulation of the complexes of $M2TM_{S31N}$ with **1**, **6**, **10** are depicted in Figure 7).

Changes in C-terminus structure-function of $M2TM_{S31N}$ and $M2TM_{WT}$ induced by V27 interactions with the adamantyl cage of amantadine variants

Furthermore it is suggested that the 10º helical kink that reduces the tilt of the C-terminal portion of the transmembrane helix in the WT is likely induced by the formation of a strong binding pocket for the aminoadamantanes. This hydrophobic pocket formed by the V27 aliphatic sidechains coupled with the aliphatic adamantyl cage of the aminoadamantanes may prevent the W41 gate from opening further defeating proton conductance. In contrast the aminoadamantanes in $M2TM_{S31N}$ included a loss of V27 lipophilic pocket and have their amino group drawn toward the N-terminus by the asparagine sidechains resulting in the presence of multiple water molecules in this region. In addition the weak binding of the amino adamantanes results in no perturbation of the helical tilt and the W41 gate can function normally.

CONCLUSIONS

This work represents a study of the binding of amantadine variants against the proton channel formed by the tetrameric structure of the influenza A M2 protein. Significantly, we focus on aminoadamantane variants of **1** binding to $M2TM_{S31N}$ compared to $M2TM_{WT}$ aiming at investigating why these variants are ineffective in blocking proton conductance of the $M2_{S31N}$ channel. The results of this effort are based on a combination of experimental techniques and MD simulations both performed in liquid crystalline lipid bilayer environments. Aminoadamantane derivatives are known to be blockers of the M2 WT protein. They are known to bind in the pore and are presumed to block proton access to the H37 tetrad that is known to shuttle protons through aqueous pore into the viral interior.[47] There are two gates that can inhibit conductance, the V27 tetrad, known as the secondary gate at the external entrance to the pore and the W41 tetrad near the exit of the pore into the viral interior, known as the primary gate. These aminoadamantane derivatives were weaker binders to $M2TM_{S31N}$ compared to $M2TM_{WT}$ as observed by a reduced influence on the protein structure and by reduced amplitude of the channel dynamics as observed by both the MD and experimental data. Moreover, these aminoadamantane derivatives were ineffective against $M2_{S31N}$ while blocking $M2_{WT}$ protein. We suggest that **1** and the similar sized analogs **2-4** lack of binding affinity and the larger sized analogs **5-8** showed weak binding affinity to $M2TM_{S31N}$ because of a lack of effective hydrophobic interactions as a result of reshaping the cavity when N31 is present which included loss of V27 lipophilic pocket. In contrast V27 interactions are present with **1-8** in $M2TM_{WT}$ pore and these ligands are effective binders to $M2TM_{WT}$. All ligands **1-8** have a tight binding for $M2TM_{WT}$ and the binding is more specific as showed by the more stringent head-ammonium group requirements in the binding pocket of $M2TM_{WT}$ than in the $M2TM_{S31N}$ according to the ITC, EP and CPE results. The weak binding of **5-8** to $M2TM_{S31N}$ was significant enough to induce observable changes in the helix tilt angles characterized by the experimental data and by the MD simulations.

It is interesting to note that the blockage of $M2TM_{WT}$ by both **1** and **5** involved a 10° kink in the TM helix and a very significant change in the helix orientation in the C-terminal half of the TM. This is likely due to the V27 side chains - adamantane hydrophobic interactions that are not possible in $M2TM_{S31N}$. While aminoadamantane ligand binding causes a kink in the C-terminal half of $M2TM_{WT}$ and a blockage for proton conductance by the M2 channel, aminoadamantane ligand interactions with $M2TM_{S31N}$ did not result in a helix kink in the TM helix and proton conductance was not blocked. While the helix kink has been associated with blockage and potential disabling the opening of W41 gate in $M2TM_{WT}$ previously[48] here, the explanation for the helix kink in the $M2TM_{WT}$ and its absence in $M2TM_{S31N}$ has been suggested to be induced by the V27 interactions with the adamantyl cage in the $M2TM_{WT}$ and the absence of such significant interactions in the $M2TM_{S31N}$.

EXPERIMENTAL METHODS

1 Synthesis of aminoadamantane ligands

The procedures applied for the synthesis of the new derivatives **8** and **10** are depicted in Schemes 2 and 3. The description of synthetic procedures for **8** and **10**, experimental details and compound characterization can be found in the Supporting Information. All compounds purity was ≥ 95% as determined by elemental analysis (see Supporting Information).

2 M2TM peptide synthesis

$M2TM_{WT}$ peptides corresponding to residues 22-46 of the Udorn (A/Udorn/307/72) sequence of M2 (C-terminally amidated SSDPLVVAASIIGILHLILWILDRL) and of the S31N mutant peptide (C-terminally amidated SSDPLVVAANIIGILHLILWILDRL) were synthesized by standard Fmoc (9-fluorenylmethoxycarbonyl) solid phase peptide synthesis using an aminomethyl polystyrene resin loaded with the amide linker and purified by reverse phase HPLC before used for the ITC experiments. Additional quantities of these peptides needed were purchased from Centic Biotec, Heildeberg, Germany. For ssNMR experiments $M2TM_{WT}$ and $M2TM_{S31N}$ (22-46) peptides with ^{15}N labeled at V28, A30 and I42 and $M2TM_{S31N}$ (22-46) peptides with ^{13}C, ^{15}N labeled at structurally important residues V27, A30[4a,5b] and N31, G34 (^{13}C,^{15}N-VANG) were synthesized using Fmoc chemistry. Fmoc-[^{15}N]-Val, Fmoc-[^{15}N]-Ala, Fmoc-[^{15}N]-Ile and Fmoc-[^{13}C,^{15}N]-Val, Fmoc-[^{13}C,^{15}N]-Ala, Fmoc-[^{13}C,^{15}N]-Ser and Fmoc-[^{13}C,^{15}N]-Gly were purchased from Cambridge Isotope Laboratory (Andover, MA). Solid-phase syntheses of M2TM peptides (0.25 mmol) were performed on an Applied Biosystems 430A peptide synthesizer as previously described.[49,50] The peptide was cleaved from the resin by the treatment with ice cold 95 % TFA, 2.5 % H_2O, 1.25 %

ethanedithiol, 1.25 % thioanisole and precipitated from TFA using ice cold ether. Following centrifugation, the supernatant was discarded and the pellet was washed with cold ether again. The precipitated peptide was dried under vacuum. A purification procedure previously described[51] and modified[50] was used. Peptide purity and identity was confirmed using ESI mass spectrometry (positive ion mode). The final peptide purity was 98 %.

3 ITC measurements of aminoadamantane ligands binding to M2TM

Binding affinities of the aminoadamantane derivatives **1-5, 6, 9, 10** for $M2TM_{S31N}$ were measured by ITC experiments[52,53] in DPC micelles at pH 8. Compounds **7**, **8** were not measured. M2TM fragments form stable tetramers at this pH, in contrast to low pH (< 6.5) conditions.[54] Furthermore, experimental data indicate that **1** binds with higher affinity at alkaline pH to M2TM, where the pore of the M2 channel is in the closed state, than at low pH, where the open state of M2TM is prevalent.[54a,2a]

All measurements were performed with a TAM 2277 (TA instrument) at pH 8 and 20 °C in a buffer of 50 mM NaH_2PO_4 and 100 mM NaCl. The peptide and the aminoadamantane derivative were dissolved in a freshly prepared DPC solution with a concentration of 13 mmol L^{-1}. Measurements against $M2TM_{WT}$ were conducted using 2 mL of 125 µM peptide (corresponding to 31.25 µM $M2TM_{WT}$ tetramer) as has been described previously.[26] For the low affinity ligands **9** and **10** a 250 µM peptide concentration was used. For $M2TM_{S31N}$ measurements the concentration of the peptide used was 167 µM, which was increased to 500 µM when **5** was tested in order to get a curve adequate for measurements. A concentration of 1.1 mM of the ligand was used for the titrant, of which 7.6 µL (equivalent to 8.4 nmol) were dispensed in the peptide/DPC solution with each injection. The time interval between two injections was set to at least 6 minutes. First injection wasn't used due to dilution effects.

Synthetic $M2TM_{S31N}$ (residues 22-46) was reconstituted in DPC micelles at pH 8 at a 1:40 monomer/DPC ratio - which guarantees the quantitative formation of M2TM tetramers[54] - by dissolving and sonicating 334 nmol of M2TM with the 40-fold amount of DPC in the aforementioned buffer system (for $M2TM_{WT}$ a 1:26 ratio was applied for the measurements of ligands **9**, **10** compared to 1:57 applied previously[26]). Solutions of the ligands in the buffer were titrated into the calorimetric cell at 20 °C. The released heat of binding was derived by subtracting the heat of dilution from the heat of reaction.[55,56]

Describing in more detail, to determine the heat of dilution ligand as well as receptor (M2TM) were dissolved in buffer containing DPC. Two reference experiments were carried out, i.e., (a) ligand was titrated into the buffer containing DPC and (b) receptor was titrated into buffer containing DPC. The obtained signals showed, that the released heat of each injection is very small and stays constant during the experiment. No interaction is detected between ligand and DPC containing buffer or receptor and DPC containing buffer, respectively. The released heat is the heat of dilution, which occurs when the two solutions are mixed. The heat of dilution was estimated for each titration experiment individually. At the end of each measurement, the receptor is titrated with the ligand being in an excess (the ratio for ligand/receptor after 19 injections is 2:1). If all binding sites are saturated, ligand can't bind to the receptor anymore. The released heat is then equivalent to the heat of dilution. As mentioned the heat of dilution is calculated as an average from the last five titration steps, when the heat is constant. This heat is take into account as Q correction. It is subtracted from all titrations steps in this measurement.

Data evaluation, including the integration of the peaks, was carried out with Digitam for Windows v4.1. The measured heat per amount of substance against the molar ratio of titrant to peptide tetramer was plotted and the affinity constants were calculated by non-linear regression of the measured heat per injection using Origin 8.0[57] and are included in Table 1. Compounds **1-8** have been measured against $M2TM_{WT}$ in a previous work (Table S1).[26] For the calculation, the concentration of the peptide was kept variable because the M2TM tetramer formation is not

complete. The fit function involves three parameters. One of them is a factor for the correction of the peptide concentration (the difference between the concentration, which has been weighted in, and the active concentration). The cell volume is fixed at 2 mL. The concentration of the ligand in the solution is known, because pure substance was weighted in and the stoichiometry of the binding of ligand to receptor was assumed to be 1:1. If these quantities are set, the concentration of active receptor is obtained by fitting the measured data points. From the calculations, it can be seen, that the concentration of active receptor is lower than the concentration of receptor that has been weighted in. The binding affinity of **1** measured against $M2TM_{WT}$ in a previous work[26] was 2.17 ± 0.52 μM and is comparable with the value of 12 μM measured using analytical ultracentrifugation[54c] and the value of 9 ± 2 μM derived based on kinetic studies in electrophysiological experiments.[2a] For the M2TM peptide investigated in this study, the solubility in the DPC micelles limits the concentration of M2TM that can be tested. Consequently, affinity constants of low affinity binders, e.g., aminoadamantanes against $M2TM_{S31N}$ and **9**, **10** against $M2TM_{WT}$ possess relatively large errors.

4 Sample preparation for solid state NMR

^{15}N-$V_{28}A_{30}I_{42}$ $M2TM_{WT}$ or $M2TM_{S31N}$ was co-dissolved in trifluoroethanol (TFE) with DMPC in a 1:30 molar ratio. (The molar ratio of 1 protein tetramer to 120 DMPC lipids was used. The molecular weight of the $M2TM_{WT}$ peptide is MW = 2729 g/mole and the lipid is MW = 678 g/mole). The solvent was removed under a stream of nitrogen gas to yield a lipid film, and then dried to remove residual organic solvent under vacuum for 12 hours. Thoroughly dried lipid film was hydrated with 10 mM HEPES buffer at pH 7.5 to form multilamellar vesicles containing M2TM in tetrameric state. This suspension was bath sonicated, dialyzed against 2L HEPES 10 mM pH 7.5 buffer for 1 day and centrifuged at 196,000xg to harvest unilamellar proteoliposomes. The pellet was re-suspended in a 1 mL aliquot of the decanted supernatant containing the ligand,

resulting in a 1:6 molar ratio of the M2TM tetramer to drug. Typically a preparation for solid state NMR would include 5 mg of protein and 37 mg of DMPC. For samples that included drug the molar ratio of drug to tetramer was 6:1. For **1** with a molecular weight of M_w = 187.5 g/mole that would mean the addition 0.52 mg for a 5 mg protein sample (There is sufficient evidence in the literature to demonstrate that M2 structure is not perturbed by drug concentration. The most obvious example in this manuscript, is the absence of structural changes in the S31N spectra in the presence of **1**) Following overnight incubation at 37°C, the pellet was deposited on 5.7x10mm glass strips (Matsunami Trading, Osaka, Japan). The bulk of the water from the sample was removed during a two day period in a 98 % relative humidity environment at 298 K. Rehydration of the slides, before stacking and sealing into a rectangular sample cell, increased the sample weight by 40-50 %. Compounds **1**, **5** were used for ssNMR experiments against $M2TM_{WT}$; compounds **1**, **5-8** were used for ssNMR experiments against $M2TM_{S31N}$; compounds **9** and **10** produce disordered lipid bilayers according to the ^{31}P spectra (not shown).

5 Solid state NMR experiments of M2TM-aminoadamananes complexes

OS ssNMR spectra

PISEMA[28] and SAMPI4[29,30] spectra were acquired at 720 MHz utilizing a low-E $^{1}H/^{15}N$ double resonance probe.[58] Acquisition took place at 303 K, above the gel to liquid crystalline phase transition temperature of DMPC lipids. Experimental parameters included a 90° pulse of 5 µs and cross-polarization contact time of 0.8-1 ms, a 4 s recycle delay and a SPINAL decoupling sequence.[58] 32 t_1 increments were obtained for the spectrum of ^{15}N-$V_{28}A_{30}I_{42}$ $M2TM_{WT}$ with compounds **1, 5** and nine t_1 for the sample of ^{15}N-$V_{28}A_{30}I_{42}$ $M2TM_{WT}$ without drug. 16-28 t_1 increments were obtained for the spectrum of ^{15}N-$V_{28}A_{30}I_{42}$ $M2TM_{S31N}$ with compounds **1, 5-8** and

nine t_1 increments for the sample of ^{15}N-$V_{28}A_{30}I_{42}$ M2TM$_{S31N}$ without drug. Spectral processing was done with NMRPIPE[59] and plotting with SPARKY. ^{15}N chemical shifts were referenced to a concentrated solution of $N_2H_8SO_4$, defined as 26.8 ppm relative to liquid ammonia.

NCA MAS spectra

^{15}N-^{13}Cα correlation experiments were performed on a Bruker Avance 600 MHz NMR Spectrometer with an NHMFL 3.2 mm low-E-field triple resonance probe.[60,61] The ^{13}C chemical shifts were referenced using the published chemical shifts of adamantane relative to DSS[62] and ^{15}N chemical shifts were calculated with IUPAC relative frequency ratios between the DSS (^{13}C) and liquid ammonia (^{15}N).[63,64] Spectra were acquired at magic angle spinning (MAS) frequency of 10-12 kHz and a calibrated sample temperature of -10 °C. 30 points were collected in the ^{15}N dimension for an acquisition time of 5-6.25 ms, while in the direct dimension the acquisition time was 10.2 ms. 92 kHz of proton decoupling was used in all experiments. To get one bond ^{15}N-^{13}C correlation a mixing time of 5 ms was used. Spectra were processed with Topspin.

6 MD simulations of M2TM-aminoadamantane complexes

Docking calculations

The ligands in their ammonium forms were built by means of Maestro 8.5[65] and were then minimized by means of Macromodel 9.6 and the MMFF94 force field[66] implemented with Macromodel 9.6 using the CG method and a distance-dependent dielectric constant of 4.0 until a convergence value of 0.0001 kJ Å^{-1} mol^{-1} was reached. The M2TM$_{WT}$-**1** complex structure (PDB ID 2KQT[4a,5b]) served as a model structure for M2TM$_{WT}$ with bound ligands. N- and C-termini of the M2TM model systems were capped by acetyl and methylamino groups. After applying the protein preparation module of Maestro, all hydrogens of the protein complex were minimized with the

AMBER* force field by means of Maestro/Macromodel 9.6 using a distance-dependent dielectric constant of 4.0. The molecular mechanics minimizations were performed with a conjugate gradient (CG) method and a threshold value of 0.0001 kJ $Å^{-1}$ mol^{-1} as the convergence criterion. The structures of the protein and ligand **1** were saved separately and were used for the subsequent docking calculations. The ligands minimized in this manner were docked into the $M2TM_{WT}$ binding site. Docking poses of the aminoadamantane derivatives **1-10** in the $M2TM_{WT}$ bound state were generated with GOLD 5.2[67,68] considering five water molecules located between ammonium group of **1** and H37 within the $M2TM_{WT}$ pore-binding site and applying the ChemPLP implemented in the software.[69,70] The option "toggle" was used to let the algorithm decide whether taking into account a water molecule or neglecting it based on an empirical desolvation penalty. The region of interest used by GOLD was defined to contain the atoms that were within ~15 Å of **1** binding site in the receptor structure. The "allow early termination" command was deactivated. For all the other parameters, GOLD default values were used. Ligands were submitted to 30 genetic algorithm runs. Ten docking poses were produced for each ligand which were visually inspected using the UCSF Chimera package.[71] The docking pose with the best ChemPLP score was used for the subsequent MD simulations with $M2TM_{WT}$ and $M2TM_{S31N}$ structures created as described below.

MD simulations

Models of $M2TM_{S31N}$-aminoadamantane complexes were generated from $M2TM_{WT}$ aminoadamantane complexes by mutating amino acids S31 to N31 with Maestro[65] and preparing the structure as described above i.e. N- and C-termini of the M2TM peptides were capped by acetyl- and methylamino groups, respectively. For N31, the side chain rotamers may have χ_1 angles -160° or -80° corresponding to N31 side chains placed at the interface between helices or inside the lumen respectively. Structures of $M2TM_{S31N}$(18-60) in DPC micelles solved by solution NMR spectroscopy show residue 31 in the helix−helix interface[72] while MAS ssNMR studies in 1,2-diphytanoyl-sn-glycero-3-phosphocholine (DPhPC) bilayers showed the side chain of the N31

residue oriented toward the pore in two helices and toward an adjacent helix in the other two, with neighboring N31 side chains close enough to form polar contacts.[37] A just-released X-ray structure show that N31 residues are oriented into the channel pore forming a hydrogen-bonding network[73] and it was suggested that this may prevent drug for entering the channel. Preliminary OS ssNMR results in liquid crystalline lipid bilayers confirm that the all four of the $M2_{S31N}$ N31 residues are oriented toward the pore. Simulations of $M2TM_{S31N}$-ligands were run a) with N31 side chains placed at the interface between helices[72] (χ_1 angle is -80°) to avoid a biased starting conformer in which N31 repel adamantane and b) with N31 pointing toward the pore in two helices (χ_1 angle is ~-160°) and toward an adjacent helix in the other two[37] (χ_1 angle is ~-80°). For comparison reasons few MD simulations with **1**, **5**, **6** were also performed with the starting structure of $M2TM_{S31N}$ having N31 residues pointing into the center of the channel pore (χ_1 angle is -160°).[73] It should be mentioned that when the starting structure has all four N31 side chains placed at the interface between helices after a few ns of simulation the side chains of at least two N31 residues change orientation pointing inside the pore lumen. This was also observed with the *apo* protein $M2TM_{S31N}$ after a few ns. Configurations with different N31 rotamers produced MD trajectories with similar behavior for aminoadamantane ligands. MD simulations were run in triplicate or more for **1**, **2**, **5**, **6** to test reproducibility of the behavior of the system.

The $M2TM_{WT}$ complexes or $M2TM_{S31N}$ complexes were embedded in a DMPC lipid bilayer extending 10 Å beyond the solutes. Complex and ligand systems were solvated using the TIP3P[74] water model. Na^+ and Cl^- ions were placed in the water phase to neutralize the systems and to reach the experimental salt concentration of 0.150 M NaCl. Membrane creation and system solvation were conducted with the "System Builder" utility of Desmond.[75,76] The $M2TM_{WT}$-**1** complex structure in the hydrated DMPC bilayer with ions included 18617 atoms.

The OPLS 2005 force field[77-79] was used to model all protein and ligand interactions, and the TIP3P model[74] was used for water. The particle mesh Ewald method (PME)[80,81] was employed to calculate long-range electrostatic interactions with a grid spacing of 0.8 Å. Van der Waals and short

range electrostatic interactions were smoothly truncated at 9.0 Å. The Nosé-Hoover thermostat[82] was utilized to maintain a constant temperature in all simulations, and the Martyna-Tobias-Klein method[82] was used to control the pressure. Periodic boundary conditions were applied (50×50×80)Å^3. The equations of motion were integrated using the multistep RESPA integrator[83] with an inner time step of 2 fs for bonded interactions and non-bonded interactions within a cutoff of 9 Å. An outer time step of 6.0 fs was used for non-bonded interactions beyond the cut-off.

Each system was equilibrated in MD simulations with a modification of the default protocol provided in Desmond, which consists of a series of restrained minimizations and MD simulations designed to relax the system, while not deviating substantially from the initial coordinates. First, two rounds of steepest descent minimization were performed with a maximum of 2000 steps with harmonic restraints of 50 kcal mol^{-1} Å^{-2} applied on all solute atoms, followed by 10000 steps of minimization without restraints. The first simulation was run for 200 ps at a temperature of 10 K in the NVT (constant number of particles, volume, and temperature) ensemble with solute heavy atoms restrained with a force constant of 50 kcal mol^{-1} Å^{-2}. The temperature was then raised during a 200 ps MD simulation to 310 K in the NVT ensemble with the force constant retained. The temperature of 310 K was used in our MD simulations in order to ensure that the membrane state is above the melting temperature state of 297 K for DMPC lipids.[84]

The heating was followed by equilibration runs. First, two stages of NPT equilibration (constant number of particles, pressure, and temperature) were performed, one with the heavy atoms of the system restrained for 1 ns and one for solvent and lipids for 10 ns, with a force constant of 10 kcal/mol/Å^2 for the harmonic constraints, respectively. A NPT simulation followed with the C_α atoms restrained for 1ns with a force constant of 2 kcal/mol/Å^2. The above-mentioned equilibration was followed by a 80 ns NPT simulation without restraints. Within this time, the total energy and the RMSD reached a plateau, and the systems were considered equilibrated.

7 Electrophysiology experiments of M2 blockage by aminoadamantanes

Electrophysiology was performed as previously described.[10a] pcDNA3 vectors encoding the full-length A/California/07/2009 (H1N1) M2 protein containing either an N31 or an S31 mutation was co-transfected with a pcDNA3 vector encoding eGFP into TSA-201 (HEK parental) cells using standard transfection protocols (Lipofectamine 2000, Life Technologies). This construct was previously annotated as A/England/195/2009 (H1N1)[10a] but is identical in amino acid sequence to A/California/07/2009 (H1N1). Macroscopic ionic currents were recorded in the whole-cell configuration from GFP-positive cells 24−48 h after transfection. Cells were perfused continuously at 3-5 mL min^{-1} with external (bath) solution containing (in mM) 150 NMG, 10 HEPES, 10 D-glucose, 2 $CaCl_2$, and 1 $MgCl_2$ buffered at pH 7.4 with HCl. For low pH (pH = 5.5) solution, HEPES was replaced by MES. Patch electrodes were pulled from thin-walled borosilicate glass (World Precision Instruments, Fl) and fire-polished before filling with standard pipet solution containing (in mM) 140 NMG, 10 EGTA, 10 MES, and 1 $MgCl_2$ buffered at pH 6.0 with HCl. Voltage-clamp experiments were performed with an Axopatch 200B amplifier (Molecular Devices, CA) connected to a Digidata 1322A 16-bit digitizer. Data were acquired with the pCLAMP8.0 software (Molecular Devices, CA) sampled at 10 kHz and low-pass-filtered at 5 kHz. Cells were held at − 40 mV. The voltage protocol consisted of a 100 ms pulse to − 80 mV followed by a 300 ms ramp to + 40 mV and a 200 ms step to 0 mV before stepping back to − 40 mV, which was repeated every 4 s. All drugs were prepared as DMSO stocks (50 or 100 mM) and diluted with external solution to desired concentrations. To measure block of M2 currents by compounds, cells were recurrently treated with pH 7.4 and pH 5.5 solutions until stable, pH-dependent inward currents were reproducibly observed, followed by treatment with compound at pH 5.5 for 2-30 min. At the end of each experiment, cells were treated with a 100 μM solution of **1**.

8 Cells and viruses

Madin-Darby canine kidney (MDCK) cells (Cat.no. RIE 328, Friedrich-Loeffler Institute, Riems, Germany) were propagated as monolayer in Eagle's minimum essential medium (EMEM) supplemented with 10 % fetal bovine serum, 1 % non-essential amino acids (NEAA), 1 mM sodium pyruvate and 2 mM L-glutamine. Amantadine-resistant WSN/33 (with N31 in M2) and its amantadine-sensitive variant WSN/33-M2-N31S[44] were used in this study. For the generation of WSN/33-M2-N31S[44] the plasmid pHW187-M2-N31 was altered by site-directed mutagenesis PCR and afterwards used as part of a plasmid set for virus recovery.[44] Both WSN/33-variants were propagated on MDCK cells in serum-free EMEM supplemented with 2 mM L-glutamine, 2 µg/mL trypsin, and 0.1 % sodium bicarbonate (test medium). Virus containing supernatant was harvested after about 48 h of incubation at 37 °C when cytopathic effect became microscopically visible. Aliquots were stored at -80 °C until use. The M2 gene identity of all recombinant viruses was verified by sequencing.

9 CPE inhibition assay of influenza A viruses by aminoadamantanes

Cytotoxicity and CPE inhibition studies were performed on two-day-old confluent monolayers of MDCK cells grown in 96-well plates as published.[46] Cytotoxicity was analyzed 72 h after compound addition (two-fold or half-log dilutions; at least two parallels per concentration; maximum concentration 100 µM). In CPE inhibition assay, 50 µL of two-fold compound dilutions in test medium and a constant multiplicity of infection of test virus (0.045 for WSN/33 and 0.04 for WSN/33-M2-N31S) in a volume of 50 µL of the test medium were added to cells. Then, plates were incubated at 37 °C with 5% CO_2 for 48 h till the untreated, infected control showed maximum cytopathic effect. Crystal violet staining and optical density determination were performed as described before to determine the percentage of antiviral activity of the tests compounds.[45,46] After

log transformation of compound concentrations, linear regression was used to determine the 50 % cytotoxic (CC_{50}) and the 50 % inhibitory concentration (IC_{50}) (Table 5). At least three independent assays were conducted to calculate the mean CC_{50} as well as IC_{50}s and their standard deviations.

SUPPORTING INFORMATION AVAILABLE

Supplementary material including detailed synthesis information, information for ITC method limitations, four Tables, snapshots of additional MD runs, RMSD plots from MD runs and relevant references. In addition Molecular Formula Strings. This material is available free of charge via the Internet at http://pubs.acs.org.

AUTHOR INFORMATION

* Corresponding author: Antonios Kolocouris (A.K.), Panepistimioupolis – Zografou, 15771Athens, Greece; Phone: (+301) 210-7274834, Fax: (+301) 210 727 4747; E-mail: ankol@pharm.uoa.gr

A.K. designed this research project. C.T and A.W contribute equally. C.T. in A.K. group performed the MD simulations and did the synthesis of the $M2TM_{S31N}$ peptide and of the new ligands **8, 10** as part of her Ph.D work. A.W. in T.C. group synthesized the labeled $M2TM_{S31N}$ peptides and did the ssNMR experiments work. K.F. and F.K. in G.G group did the ITC measurements. I.T. in D.F. group did the EP experiments. A.H. in M.S. group performed CPE inhibitory assays with A/WSN/33 and A/WSN/33-M2-N31S viruses. A.K. wrote the manuscript and T. C. revised it.

ACKNOWLEDGEMENTS

The NMR experiments were performed at the National High Magnetic Field Laboratory, which is supported by a National Science Foundation Cooperative Agreement (DMR-1157490) with the State of Florida. A.K. thanks Chiesi Hellas for supporting the Ph.D research of C.T. A.K. also thanks Harris Ioannidis and Antonios Drakopoulos (previous M.Sc students) for running few preliminary MD runs. This work was in part supported by NIH Grant AI023007 and a Grand Challenges Stars in Global Health grant to I.T. and D.F. D.F. thanks Daniel Kwan for technical assistance.

AB BREVIATIONS

ssNMR, solid state NMR; NCA, ^{15}N-^{13}Cα; MAS, Magic Angle Spinning; OS, Oriented Sample; M2TM, M2 transmembrane domain; MD, molecular dynamics; CPE, cytopathic effect; DMPC, 1,2-dimyristoyl-sn-glycero-3-phosphocholine; DPhPC, 1,2-diphytanoyl-sn-glycero-3-phosphocholine; ITC, Isothermal Titration Calorimetry; EP, electrophysiology; WT:, wild-type; MM/PBSA, Molecular Mechanics Poisson-Boltzmann Surface Area; BAR, Bennett acceptance ratio; HEK, Human Embryonic Kidney; PMF, Potential of Mean Force.

REFERENCES

1. Helenius, A. Unpacking the incoming influenza virus. *Cell* **1992**, *69*, 577-578.

2. (a) Wang, C.; Takeuchi, K.; Pinto, L. H.; Lamb, R. A. Ion channel activity of influenza A virus M2 protein: characterization of the amantadine block. *J. Virol.* **1993,** *67*, 5585-5594; (b) Chizhmakov, I. V.; Geraghty, F. M.; Ogden, D. C.; Hayhurst, A.; Antoniou, M.; Hay, A. J. Selective proton permeability and pH regulation of the influenza virus M2 channel expressed in mouse erythroleukaemia cells. *J. Physiol.* **1996,** *494*, 329-336.

3. Hayden, F. G. Clinical applications of antiviral agents for chemophrophylaxis and therapy of respiratory viral infections. *Antiviral Res.* **1985,** 229-239.

4. (a) Hu, J.; Asbury, T.; Achuthan, S.; Li, C.; Bertram, R.; Quine, J. R.; Fu, R.; Cross, T. A. Backbone structure of the amantadine-blocked trans-membrane domain M2 proton channel from influenza A virus. *Biophys. J.* **2007,** *92*, 4335-4343; (b) Hu, J.; Fu, R.; Cross, T. A. The chemical and dynamical influence of the anti-viral drug amantadine on the M2 proton channel transmembrane domain. *Biophys. J.* **2007,** *93*, 276-283.

5. (a) Stouffer, A. L.; Acharya, R.; Salom, D.; Levine, A. S.; Di Costanzo, L.; Soto, C. S.; Tereshko, V.; Nanda, V.; Stayrook, S.; DeGrado, W. F. Structural basis for the function and inhibition of an influenza virus proton channel. *Nature* **2008,** *451*, 596-599; (b) Cady, S. D.; Schmidt-Rohr, K.; Wang, J.; Soto, C. S.; Degrado, W. F.; Hong, M. Structure of the amantadine binding site of influenza M2 proton channels in lipid bilayers. *Nature* **2010,** *463*, 689-692; (c) Cady, S. D.; Wang, J.; Wu, Y.; DeGrado, W. F.; Hong, M. Specific binding of adamantane drugs and direction of their polar amines in the pore of the influenza M2 transmembrane domain in lipid bilayers and dodecylphosphocholine micelles determined by NMR spectroscopy. *J. Am. Chem. Soc.* **2011,** *133*, 4274-4284; (d) Jing, X.; Ma, C.; Ohigashi, Y.; Oliveira, F. A.; Jardetzky, T. S.; Pinto, L. H.; Lamb, R. A., Functional studies indicate amantadine binds to the pore of the influenza A virus M2 proton-selective ion channel. *Proc. Natl. Acad. Sci. U. S. A.* **2008,** *105*, 10967-10972. (e) Pielak, R. M.;

Oxenoid, K.; Chou, J. J. Structural investigation of rimantadine inhibition of the AM2-BM2 chimera channel of influenza viruses. *Structure* **2011,** *19*, 1655–1663.

6. Bright, R. A.; Medina, M. J.; Xu, X.; Perez-Oronoz, G.; Wallis, T. R.; Davis, X. M.; Povinelli, L.; Cox, N. J.; Klimov, A. I. Incidence of adamantane resistance among influenza A (H3N2) viruses isolated worldwide from 1994 to 2005: a cause for concern. *Lancet* **2005,** *366*, 1175-1181.

7. (a) Bright, R. A.; Shay, D. K.; Shu, B.; Cox, N. J.; Klimov, A. I. Adamantane resistance among influenza A viruses isolated early during the 2005-2006 influenza season in the United States. *J. Am. Med. Assoc.* **2006,** *295*, 891-894; (b) Lan, Y.; Zhang, Y.; Dong, L.; Wang, D.; Huang, W.; Xin, L.; Yang, L.; Zhao, X.; Li, Z.; Wang, W.; Li, X.; Xu, C.; Guo, J.; Wang, M.; Peng, Y.; Gao, Y.; Guo, Y.; Wen, L.; Jiang, T.; Shu, Y. A comprehensive surveillance of adamantane resistance among human influenza A virus isolated from mainland China between 1956 and 2009. *Antivir. Ther.* **2010,** *15*, 853-859.

8. High levels of adamantane resistance among influenza A (H3N2) viruses and interim guidelines for use of antiviral agents--United States, 2005-06 influenza season. *MMWR Morb. Mortal Wkly Rep.* **2006,** *55*, 44-46.

9. See for example: (a) Kolocouris, N.; Foscolos, G. B.; Kolocouris, A.; Marakos, P.; Pouli, N.; Fytas, G.; Ikeda, S.; De Clercq, E. Synthesis and antiviral activity evaluation of some aminoadamantane derivatives. *J. Med. Chem.* **1994,** *37*, 2896-2902. (b) Kolocouris, N.; Kolocouris, A.; Foscolos, G. B.; Fytas, G.; Neyts, J.; Padalko, E.; Balzarini, J.; Snoeck, R.; Andrei, G.; De Clercq, E. Synthesis and antiviral activity evaluation of some new aminoadamantane derivatives. 2. *J. Med. Chem.* **1996,** *39*, 3307-3318. (c) Kolocouris, A.; Spearpoint, P.; Martin, S. R.; Hay, A. J.; Lopez-Querol, M.; Sureda, F. X.; Padalko, E.; Neyts, J.; De Clercq, E. Comparisons of the influenza virus A M2 channel binding affinities, anti-influenza virus potencies and NMDA antagonistic activities of 2-alkyl-2-aminoadamantanes and analogues. *Bioorg. Med. Chem. Lett.* **2008**, *18*, 6156-6160.

10. (a) Kolocouris, A.; Tzitzoglaki, C.; Johnson, F. B.; Zell, R.; Wright, A. K.; Cross, T. A.; Tietjen, I.; Fedida, D.; Busath, D. D. Aminoadamantanes with persistent in vitro efficacy against H1N1 (2009) influenza A. *J. Med. Chem.* **2014**, *57*, 4629−4639. (b) Torres, E.; Fernández, R.; Miquet, S. P.; Font-Bardia, M.; Vanderlinden, E.; Naesens, L.; Vázquez, S. Synthesis and anti-influenza A virus activity of 2,2-dialkylamantadines and related compounds. *ACS Med. Chem. Lett.* **2012,** *3*, 1065−1069. (c) Torres, E.; Duque, M. D.; Vanderlinden, E.; Ma, C.; Pinto, L. H.; Camps, P.; Froeyen, M.; Vazquez, S.; Naesens, L. Role of the viral hemagglutinin in the anti-influenza virus activity of newly synthesized polycyclic amine compounds. *Antiviral Res.* **2013**, *99*, 281–291.

11. Yi, M.; Cross, T. A.; Zhou, H.-X. A secondary gate as a mechanism for inhibition of the M2 proton channel by amantadine. *J. Phys. Chem. B* **2008**, *112*, 7977-7979.

12. Laohpongspaisan, C.; Rungrotmongkol, T.; Intharathep, P.; Malaisree, M.; Decha, P.; Aruksakunwong, O.; Sompornpisut, P.; Hannongbua, S. Why amantadine loses its function in influenza M2 mutants: MD Simulations. *J. Chem. Inf. Model.* **2009**, *49*, 847–852.

13. Khurana, E.; Devane, R. H.; Dal Peraro, M.; Klein, M. L. Computational study of drug binding to the membrane-bound tetrameric M2 peptide bundle from influenza A virus. *Biochim. Biophys. Acta* **2011**, *1808*, 530-537.

14. Wang, J.; Ma, C.; Fiorin, G.; Carnevale, V.; Wang, T.; Hu, F.; Lamb, R. A.; Pinto, L. H.; Hong, M.; Klein, M. L.; DeGrado, W. F. Molecular dynamics simulation directed rational design of inhibitors targeting drug-resistant mutants of influenza A virus M2. *J. Am. Chem. Soc.* **2011**, *133*, 12834-12841.

15. Gu, R.-X.; Liu, L. A.; Wang, Y.-H.; Xu, Q.; Wei, D.-Q. Structural comparison of the wild-type and drug-resistant mutants of the influenza A M2 proton channel by molecular dynamics simulations *J. Phys. Chem. B* **2013**, *117*, 6042-6051.

16. Alhadeff, R.; Assa, D.; Astrahan, P. Krugliak, M.; Arkin, I. T. Computational and experimental analysis of drug binding to the influenza M2 channel. *Biochim. Biophys. Acta* **2014,** *1838*, 1068–1073.

17. (a) Gleed, M. L.; Busath, D. D. Why bound amantadine fails to inhibit proton conductance according to simulations of the drug-resistant influenza A M2 (S31N). *J. Phys. Chem. B* **2015,** *119*, 1225-12231. (b) Gleed, M. L.; Ioannidis, H.; Kolocouris, A.; Busath, D. D. Resistance-mutation (N31) effects on drug orientation and channel hydration in amantadine-bound influenza A M2. *J. Phys. Chem. B.* **2015**, *119*, 11548-11559.

18. Llabres, S.; Juarez-Jimenez, J.; Masetti, M.; Leiva, R.; Vazquez, S.; Gazzarrini, S.; Moroni, A.; Cavalli, A,; Luque, F. J. Mechanism of the pseudoirreversible binding of amantadine to the M2 proton channel. *J. Am. Chem. Soc.*, **2016**, *138*, 15345–15358.

19. Gianti, E.; Carnevale, V.; DeGrado, W. F.; Klein, M. L.; Fiorin, G., Hydrogen-bonded water molecules in the M2 channel of the influenza A virus guide the binding preferences of ammonium-based inhibitors. *J. Phys. Chem. B* **2015**, *119*, 1173-1183.

20. (a) Andreas, L.B.; Barnes, A.B.; Corzilus, B.; Chou, J.J.; Miller, E.A.; Caporini, M.; Rosay, M.; Griffin, R.G. Dynamic nuclear polarization study of inhibitor binding to the $M2_{18–60}$ proton transporter from influenza A *Biochemistry* **2013**, *52*, 2774-2782. (b) Andreas, L. B.; Eddy, M. T.; Pielak, R. M.; Chou, J.; Griffin, R. G. Magic angle spinning NMR investigation of influenza A M2(18-60): support for an allosteric mechanism of inhibition. *J. Am. Chem. Soc.* **2010**, *132*, 10958-10960.

21. Wright, A. K.; Batsomboon, P.; Dai, J.; Hung, I.; Zhou, H.-X.; Dudley, G. B.; Cross, T. A. Differential binding of rimantadine enantiomers to influenza A M2 proton channel. *J. Am. Chem. Soc.* **2016**, *138*, 1506-1509.

22. Rey-Carrizo, M.; Barniol-Xicota, M.; Ma, C.; Frigolé-Vivas, M.; Torres, E.; Naesens, L.; Llabrés, S.; Juárez-Jiménez, J.; Luque, F. J.; DeGrado, W. F.; Lamb, R. A.; Pinto, L. H.; Vázquez, S. Easily Accessible Polycyclic Amines that Inhibit the Wild-Type and Amantadine-Resistant Mutants of the M2 Channel of Influenza A Virus. *J. Med. Chem.* **2014**, *57*, 5738−5747.

23. (a) Zhao, X.; Jie, Y.; Rosenberg, M. R.; Wan, J.; Zeng, S.; Cui, W.; Xiao, Y.; Li, Z.; Tu, Z.; Casarotto, M. G.; Hu, W. Design and synthesis of pinanamine derivatives as anti-influenza A M2

ion channel inhibitors. *Antiviral Res.* **2012**, *96*, 91-99; (b) Wang, J.; Wu, Y.; Ma, C.; Fiorin, G.; Pinto, L. H.; Lamb, R. A.; Klein, M. L.; Degrado, W. F. Structure and inhibition of the drug-resistant S31N mutant of the M2 ion channel of influenza A virus. *Proc. Natl. Acad. Sci. U. S. A.* **2013**, *110*, 1315-1320. (c) Wang, J.; Ma, C.; Jo, H.; Canturk, B.; Fiorin, G.; Pinto, L. H.; Lamb, R. A.; Klein, M. L.; Degrado, W. F. Discovery of novel dual inhibitors of wild-type and the most prevalent drug-resistant mutant, S31N, of M2 proton channel from influenza A virus. *J. Med. Chem.* **2013**, *56*, 2804-2812. (d) Wu, Y.; Canturk, B.; Jo, H.; Ma, C.; Gianti, E.; Klein, M.. L.; Pinto, L. H.; Lamb, R. A.; Fiorin, G.; Wang, J.; DeGrado, W. F. Flipping in the pore: discovery of dual inhibitors that bind in different orientations to the wild-type versus the amantadine-resistant S31N mutant of the influenza A virus M2 proton channel. *J. Am. Chem. Soc.* **2014**, 136, 17987–17995.

24. Williams, J. K.; Tietze, D.; Wang, J.; Wu, Y.; DeGrado, W. F.; Hong. M. Drug-induced conformational and dynamical changes of the S31N mutant of the influenza M2 proton channel investigated by solid-state NMR. *J. Am. Chem. Soc.* **2013**, *135*, 9885-9897.

25. Homeyer, N.; Ioannidis, H.; Kolarov, F.; Gauglitz, G.; Zikos, C.; Kolocouris, A.; Gohlke, H. Interpreting thermodynamic profiles of aminoadamantane compounds inhibiting the M2 proton channel of influenza A by free energy calculations. *J. Chem. Inf. Model.* **2016**, *56*, 110−126.

26. Ioannidis, H.; Drakopoulos, A.; Tzitzoglaki, C.; Homeyer, N.; Kolarov, F.; Gkeka, P.; Freudenberger, K.; Liolios, C.; Gauglitz, G.; Cournia, Z.; Gohlke, H.; Kolocouris, A. Alchemical free energy calculations and isothermal titration calorimetry measurements of aminoadamantanes bound to the closed state of influenza A/M2TM. *J. Chem. Inf. Model.* **2016**, *56*, 862–876.

27. Gkeka, P.; Eleftheratos, S.; Kolocouris, A.; Cournia, Z. Free energy calculations reveal the origin of binding preference for aminoadamantane blockers of influenza A/M2TM pore. *J. Chem. Theory Comput.* **2013**, *9*, 1272-1281.

28. (a) Wu, C. H.; Ramamoorthy, A.; Opella, S. J. High-resolution heteronuclear dipolar solid-state NMR spectroscopy. *J. Magn. Reson.* **1994,** *109*, 270-272. (b) Ahuja, S.; Jahr, N.; Im, S.-C.; Vivekanandan, S.; Popovych, N.; Le Clair, S. V.; Huang, R.; Soong, R.; Xu, J.; Yamamoto, K.;

Nanga, R.P.; Bridges, A.; Waskell, L.; Ramamoorthy, A. A model of the membrane-bound cytochrome b5-cytochrome P450 complex from NMR and mutagenesis data. *J. Biol. Chem.* **2013**, *288*, 22080-22095.

29. Nevzorov, A.A.; Opella, S.J. Selective averaging for high-resolution solid-state NMR spectroscopy of aligned samples. *J. Magn. Reson.* **2007**, *185*, 59-70.

30. De Simone, A.; Mote, K. R.; Veglia, G. Structural dynamics and conformational equilibria of SERCA regulatory proteins in membranes by solid-state NMR restrained simulations. *Biophys. J.* **2014**, *106*, 2566-2576.

31. Rühmann, E. H.; Rupp, M.; Betz, M.; Heine, A.; Klebe, G. Boosting affinity by correct ligand preorganization for the S2 pocket of thrombin: a study by isothermal titration calorimetry, molecular dynamics, and high-resolution crystal structures. *ChemMedChem* **2016**, *11*, 309-319.

32. Ma, C.; Polishchukb, A. L.; Ohigashia, Y.; Stouffer, A. L.; Schon, A.; Magavernb, E.; Jing, X.; Lear, J. D.; Freirec, E.; Lamb, R. A.; DeGrado, W. F.; Pinto, L. H. Identification of the functional core of the influenza A virus A/M2 proton-selective ion channel. *Proc. Natl. Acad. Sci. U. S. A.* **2009**, *106*, 12283-12288.

33. Rosenberg, M. R.; Casarottol, M. G. Coexistence of two adamantane binding sites in the influenza A M2 ion channel. *Proc. Natl. Acad. Sci. U. S. A.* **2010**, *107*, 13866-13871.

34. Marassi, F.M.; Opella, S.J. A solid-state NMR index of helical membrane protein structure and topology. *J. Magn. Reson.* **2000**, *144*, 150-155.

35. Wang, J.; Denny, J.; Tian, C.; Kim, S.; Mo, Y.; Kovacs, F.; Song, Z.; Nishimura, K.; Gan, Z.; Fu, R.; Quine, J. R.; Cross, T. A. Imaging membrane protein helical wheels. *J. Magn. Reson.* **2000,** *144*, 162-167.

36. Li, C.; Qin, H.; Gao, F. P.; Cross, T. A. Solid-state NMR characterization of conformational plasticity within the transmembrane domain of the influenza A M2 proton channel. *Biochim. Biophys. Acta* **2007,** *1768*, 3162-3170.

37. Andreas, L. B.; Eddy, M. T.; Chou, J. J.; Griffin, R. G. Magic-angle-spinning NMR of the drug resistant S31N M2 proton transporter from influenza A. *J. Am. Chem. Soc.* **2012**, *134*, 7215–7218.

38. Andreas, L. B.; Reese, M.; Eddy, M. T.; Gelev, V.; Ni, Q.-Z,; Miller, E. A.; Emsley, L.; Pintacuda, G.; Chou, J. J.; Griffin, R. G. Structure and mechanism of the influenza A $M2_{18-60}$ dimer of dimers. *J. Am. Chem. Soc.* **2015**, *137*, 14877–14886.

39. (a) Cady, S. D.; Luo, W. B.; Hu, F.; Hong, M. Structure and function of the influenza M2 proton channel. *Biochemistry* **2009**, *48*, 7356–7364. (b) Cady, S. D.; Hong, M. Effects of amantadine binding on the dynamics of bilayer-bound influenza A M2 transmembrane peptide studied by NMR relaxation. *J. Biomol. NMR* **2009**, *45*, 185–196. (c) Hu, F.; Luo, W.; Cady, S. D.; Hong, M. Conformational plasticity of the influenza A M2 transmembrane helix in lipid bilayers under varying pH, drug binding and membrane thickness. *Biochim. Biophys. Acta.* **2011**, *1808*, 415–423.

40. Cristian, L.; Lear, J. D.; DeGrado, W. F. Use of thiol-disulfide equilibria to measure the energetics of assembly of transmembrane helices in phospholipid bilayers. *Proc. Natl. Acad. Sci. U. S. A.* **2003**, *100*, 14772-14777.

41. Cady, S.; Wang, T.; Hong, M. Membrane-dependent effects of a cytoplasmic helix on the structure and drug binding of the influenza virus M2 protein. *J. Am. Chem. Soc.* **2011**, *133*, 11572–11579.

42. Saotome, K.; Duong-Ly, K.; Howard, K.P. Influenza A M2 protein conformation depends on choice of model membrane. *Biopolymers* **2015**, *104*, 405-411.

43. (a) Chizhmakov, I. V.; Geraghty, F. M.; Ogden, D. C.; Hayhurst, A.; Antoniou, M.; Hay, A. J. Selective proton permeability and pH regulation of the influenza virus M2 channel expressed in mouse erythroleukaemia cells. *J. Physiol.* **1996**, *494*, 329−336. (b) Balannik, V.; Carnevale, V.; Fiorin, G.; Levine, B.. G.; Lamb, R. A.; Klein, M. L.; DeGrado, W. F.; L Pinto, L. H. Functional studies and modeling of pore-lining residue mutants of the influenza A virus M2 ion channel. *Biochemistry* **2010**, *49*, 696−708. (c) Duque, M. D.; Ma, C.; Torres, E.; Wang, J.; Naesens, L.;

Juarez-Jimenez, J.; Camps, P.; Luque, F. J.; DeGrado, W. F.; Lamb, R. A.; Pinto, L. H.; Vazquez, S. Exploring the size limit of templates for inhibitors of the M2 ion channel of influenza A virus. *J. Med. Chem.* **2011,** *54*, 2646-2457.

44. Schade, D.; Kotthaus, J.; Riebling, L.; Kotthaus, J.; Müller-Fielitz, H.; Raasch, W.; Hoffmann, A.; Schmidtke, M.; Clement, B.; Zanamivir Amidoxime- and N-Hydroxyguanidine-Based Prodrug Approaches to Tackle Poor Oral Bioavailability. *J. Pharm. Sci.* **2015**, *104*, 3208-3219.

45. Torres, E.; Duque, M. D.; Vanderlinden, E.; Ma, C.; Pinto, L. H.; Camps, P.; Froeyen, M.; Vázquez, S.; Naesens, L. Role of the viral hemagglutinin in the anti-influenza virus activity of newly synthesized polycyclic amine compounds. *Antiviral Res.* **2013**, *99*, 281.

46. Schmidtke, M.; Schnittler, U.; Jahn, B.; Dahse, H.-M.; Stelzner, A. A rapid assay for evaluation of antiviral activity against coxsackie virus B3, influenza virus A, and herpes simplex virus type 1. *J. Virol. Methods* **2001**, *95*, 133-143.

47. Miao, Y.; Fu, R.; Zhou, H. X.; Cross, T. A. Dynamic short hydrogen bonds in histidine tetrad of full-length M2 proton channel reveal tetrameric structural heterogeneity and functional mechanism. *Structure* **2015**, *23*, 2300-2308.

48. Yi, M.; Cross, T. A.; Zhou, H. X. Conformational heterogeneity of the M2 proton channel and a structural model for channel activation. *Proc. Natl. Acad. Sci. U. S. A.* **2009**, *106*, 13311-13316.

49. Kovacs, F. A.; Cross, T. A. Transmembrane four-helix bundle of influenza A M2 protein channel: structural implications from helix tilt and orientation. *Biophys. J.* **1997,** *73*, 2511-2517.

50. Kolocouris, A.; Zikos, C.; Broadhurst, R. W. ^{19}F NMR detection of the complex between amantadine and the receptor portion of the influenza A M2 ion channel in DPC micelles. *Bioorg. Med. Chem. Letters* **2007**, *17*, 3947–3952.

51. Hansen, R. K.; Broadhurst, R. W.; Skelton, P. C.; Arkin, I. T. Hydrogen/deuterium exchange of hydrophobic peptides in model membranes by electrospray ionization mass spectrometry. *J. Am. Soc. Mass Spectr.* **2002**, *13*, 1376-87.

52. Ladbury, J. E.; Klebe, G.; Freire, E. Adding calorimetric data to decision making in lead discovery: a hot tip. *Nat. Rev. Drug Discov.* **2010**, *9*, 23-27.

53. Perozzo, R.; Folkers, G.; Scapozza, L. Thermodynamics of protein-ligand interactions: history, presence, and future aspects. *J. Recept. Signal Transduct. Res.* **2004**, *24*, 1-52.

54. (a) Salom. D.; Hill, B. R.; Lear, J. D.; DeGrado, W. F. pH-dependent tetramerization and amantadine binding of the transmembrane helix of M2 from the influenza A virus. *Biochemistry* **2000**, *39*, 14160–14170. (b) Stouffer, A. L.; Ma, C.; Cristian, L.; Ohigashi, Y.; Lamb, R. A.; Lear, J. D.; Pinto, L. H.; DeGrado, W. F. The interplay of functional tuning, drug resistance, and thermodynamic stability in the evolution of the M2 proton channel from the influenza A virus. *Structure* **2008**, *16*, 1067-1076. (c) Stouffer, A. L.; Nanda, V.; Lear, J. D.; DeGrado, W. F. Sequence determinants of a transmembrane proton channel: an inverse relationship between stability and function. *J. Mol. Biol.* **2005,** *347*, 169-179.

55. Wiseman, T., Willison, S., Brandts, J.F., Lin, L.-N. Rapid measurement of binding contstants and heats of binding using a new titration calorimeter *Anal. Biochem.* **1989**, *179* 131-137.

56. Doyle, M. L. Characterization of binding interactions by isothermal titration calorimetry. *Curr. Opin. Biotech.* **1997**, *8*, 31-35.

57. *Origin 8.1G SR1*, v8.1.13.88; OriginLab Corporation, Northampton, MA, USA: **2009**.

58. Fung, B. M.; Khitrin, A. K.; Ermolaev, K. An improved broadband decoupling sequence for liquid crystals and solids. *J. Magn. Reson.* **2000,** *142*, 97-101.

59. Delaglio, F.; Grzesiek, S.; Vuister, G. W.; Zhu, G.; Pfeifer, J.; Bax, A. NMRPipe: a multidimensional spectral processing system based on UNIX pipes. *J. Biomol. NMR* **1995,** *6*, 277-293.

60. Gorkov, P. L.; Chekmenev, E. Y.; Li, C.; Cotten, M.; Buffy, J. J.; Traaseth, N. J.; Veglia, G.; Brey, W. W. Using low-E resonators to reduce RF heating in biological samples for static solid-state NMR up to 900 MHz. *J. Magn. Reson.* **2007**, *185*, 77-93.

61. McNeill, S. A., P. L. Gorkov, K. Shetty, W. W. Brey, and J. R. Long. A low-E magic angle spinning probe for biological solid state NMR at 750 MHz. *J. Magn. Reson.* **2009**, *197*, 135-144.

62. Morcombe, C. R., Zilm, K. W. Chemical shift referencing in MAS solid state NMR. *J. Magn. Reson*. **2003**, *162*, 479-486.

63. Markley, J. L., Bax, A.; Arata, Y.; Hilbers, C. W.; Kaptein, R.; Sykes, B. D.; Wright, P. E.; Wüthrich, K. Recommendations for the presentation of NMR structures of proteins and nucleic acids. *J. Mol. Biol.* **1998**, *280*, 933-952.

64. Harris, R. K.; Becker, E. D.; Cabral de Menezes, S. M.; Goodfellow, R.; Granger, P. NMR nomenclature: nuclear spin properties and conventions for chemical shifts. IUPAC recommendations 2001. *Solid State Nucl. Magn. Reson.* **2002**, *22*, 458-483.

65. *Maestro*, version 8.5; Schrodinger, Inc.: New York, NY, **2008**.

66. (a) Halgren, T. A. Merck molecular force field. V. Extension of MMFF94 using experimental data, additional computational data, and empirical rules. *J. Comput. Chem.* **1996**, *17*, 616-641. (b) Halgren, T. A. MMFF VII. Characterization of MMFF94, MMFF94s, and other widely available force fields for conformational energies and for intermolecular-interaction energies and geometries. *J. Comp. Chem.* **1999**, *20*, 730-748.

67. Jones, G.; Willett, P.; Glen, R. C.; Leach, A. R.; Taylor, R. Development and validation of a genetic algorithm for flexible docking. *J. Mol. Biol.* **1997**, *267*, 727-748.

68. Verdonk, M. L.; Chessari, G.; Cole, J. C.; Hartshorn, M. J.; Murray, C. W.; Nissink, J. W.; Taylor, R. D.; Taylor, R. Modeling water molecules in protein-ligand docking using GOLD. *J. Med. Chem.* **2005**, *48*, 6504-6515. (c) Korb, O.; Stützle, T.; Exner, T. E. Empirical scoring functions for advanced protein-ligand docking with PLANTS. *J. Chem. Inf. Model.* **2009**, *49*, 84-96.

69. Mooij, W. T.; Verdonk, M. L. General and targeted statistical potentials for protein-ligand interactions. *Proteins: Struct., Funct., Bioinf.* **2005**, *61*, 272-287.

70. Korb, O.; Stützle, T.; Exner, T. E. Empirical scoring functions for advanced protein-ligand docking with PLANTS. *J. Chem. Inf. Model.* **2009**, *49*, 84-96.

71. Pettersen, E. F.; Goddard, T. D.; Huang, C. C.; Couch, G. S.; Greenblatt, D. M.; Meng, E. C.; Ferrin, T. E. UCSF Chimera--a visualization system for exploratory research and analysis. *J. Comput. Chem.* **2004**, *25*, 1605-1612.

72. Pielak, R. M.; Schnell, J. R.; Chou, J. J. Mechanism of drug inhibition and drug resistance of influenza A M2 channel. *Proc. Natl. Acad. Sci. U. S. A*. **2009**, *106*, 7379-7384.

73. Thomaston, J. L.; DeGrado, W. F. Crystal structure of the drug-resistant S31N influenza M2 proton channel. *Protein Sci.* **2016**, *25*, 1551-1554.

74. Jorgensen, W. L.; Chandrasekhar, J.; Madura, J. D.; Impey, R. W.; Klein, M. L. Comparison of simple potential functions for simulating liquid water. *J. Chem. Phys.* **1983**, *79*, 926-935.

75. (a) *Desmond Molecular Dynamics System*, version 3.0; D. E. Shaw Research: New York, NY, **2011**. (b) *Desmond Molecular Dynamics System*, version 3.1; D. E. Shaw Research: New York, NY, **2012**. (c) Bowers, K. J.; Chow, E.; Xu, H.; Dror, R. O.; Eastwood, M. P.; Gregersen, B. A.; Klepeis, J. L.; Kolossvary, I.; Moraes, M. A.; Sacerdoti, F. D.; Salmon, J. K.; Shan, Y.; Shaw, D. E. Scalable algorithms for molecular mynamics simulations on commodity clusters. In *Proceedings of the ACM/IEEE Conference on Supercomputing (SC06)*, Tampa, Florida, **2006**.

76. *Maestro-Desmond Interoperability Tools*, version 3.1; Schrodinger: New York, NY, **2012**.

77. (a) Jorgensen, W. L.; Maxwell, D. S.; Tirado-Rives, J. Development and testing of the OPLS all-atom force field on conformational energetics and properties of organic liquids. *J. Am. Chem. Soc.* **1996**, *118*, 11225-11236. (b) Rizzo, R. C.; Jorgensen, W. L. OPLS all-atom model for amines: resolution of the amine hydration problem. *J. Am. Chem. Soc.* **1999**, *121*, 4827–4836.

78. Kaminski, G.; Friesner, R. A.; Tirado-Rives, J.; Jorgensen, W. L. Evaluation and reparametrization of the OPLS-AA force field for proteins via comparison with accurate quantum chemical calculations on peptides. *J. Phys. Chem. B* **2001**, *105*, 6474-6487.

79. Shivakumar, D.; Williams, J.; Wu, Y.; Damm, W.; Shelley, J.; Sherman, W. Prediction of absolute solvation free energies using molecular dynamics free energy perturbation and the OPLS force field. *J. Chem. Theory Comput.* **2010**, *6*, 1509–1519.

80. Darden, T.; York, D.; Pedersen, L. Particle mesh Ewald: an N log(N) method for Ewald sums in large systems *J. Chem. Phys.* **1993**, *98*, 10089-10092.

81. Essmann, U.; Perera, L.; Berkowitz, M. L.; Darden, T.; Lee, H.; Pedersen, L. G. A Smooth particle mesh Ewald method. *J. Chem. Phys.* **1995**, *103*, 8577-8593.

82. Martyna, G. J. T., D. J.; Klein, M. L. Constant-pressure molecular-dynamics algorithms. *J. Chem. Phys.* **1994**, *101*, 4177-4189.

83. Humphreys, D. D.; Friesner, R. A.; Berne, B. J. A multiple-time-step molecular-dynamics algorithm for macromolecules. *J. Phys. Chem.* **1994,** *98*, 6885-6892.

82. Koynova, R.; Caffrey, M. Phases and phase transitions of the phosphatidylcholines. *Biochim. Biophys. Acta* **1998**, *1376*, 91-145.

SCHEME AND FIGURE CAPTIONS

Scheme 1. Structures of aminoadamantane derivatives **1-10**.

Scheme 2. Synthesis of 1´-methylspiro[pyrrolidine-2,2′-adamantane] **8**.

Scheme 3. Synthesis of 1-(1-adamantyl)cyclohexanamine **10**.

Figure 1. *Amt* (**1**) orients toward the protein C-terminus in $M2TM_{WT}$ and toward the protein N-terminus in $M2TM_{S31N}$. Superposition of final snapshots, constant temperature and pressure molecular dynamics simulations at 310 K of **1** in complex with S31 or N31 M2 [PDB ID: 2KQT] in 150 mM NaCl, water, and DMPC lipid. **1** and waters are shown in yellow-green and purple in WT and S31N respectively. Two of four M2TM backbones are shown as green ribbons. In the S31 case, the ammonium group of **1** is projecting toward the C-terminus and hydrogen bonding with four water molecules. In the N31 case, the adamantane cage (purple) is lower, and the amantadine amine projects toward the N-terminus and hydrogen bonds with the one N31 side chain and a water molecule.

Figure 2. Superimposed PISEMA spectra of the $M2TM_{WT}$ (residues 22-46), ^{15}N-labeled at V28, A30, and I42, in DMPC lipid bilayers uniformly aligned on glass slides with (red) and without (black) compound **1** (**A**) and compound **5** (**B**). Assignments without drug were made based on the known structure and spectra of $M2TM_{WT}$.[36] Assignments with drug follow the rotational orientation of the helices. Change in the resonance frequencies of the ^{15}N-labeled backbone amide sites are indicated with black arrows. All spectra were collected at 720 MHz, pH 7.5, 303K. The molar ratio of lipid/protein was 30:1. PISA wheels are drawn for helix tilts of 22° and 32° for the N- and C-terminal residues respectively when the drugs are bound.

Figure 3. Superimposed PISEMA spectra of the $M2TM_{S31N}$, ^{15}N-labeled at residues V28, A30, and I42, in DMPC lipid bilayers uniformly aligned on glass slides with (red) and without (black) compound **1** (**A**) and compound **5** (**B**). Assignments without drug were made based on the known structure and spectra of $M2TM_{WT}$.[36] Assignments with drug follow the rotational orientation of the helices. Theoretical PISA wheel calculated for an ideal helix [(ϕ,φ)] = (-60°, -45°)] with a 33° tilt angle relative to the bilayer normal is superimposed on $M2TM_{S31N}$ resonance frequencies, which are shifted after compound **5** addition. All spectra were collected at 720 MHz, pH 7.5, 303K. The molar ratio of lipid/protein was 30:1.

Figure 4. Superimposed PISEMA spectra of the $M2TM_{S31N}$ (residues 22-46), ^{15}N labeled at residues V28, A30, and I42, in DMPC bilayers uniformly aligned on glass slides with (red) and without (black) **6**, **7**, and **8** (Figures 4 A-C respectively). Assignments without drug were made based on the known structure and spectra of $M2TM_{WT}$.[36] Assignments with drug follow the rotational orientation of the helices. Theoretical PISA wheels calculated for an ideal helix [(ϕ,φ)] = (-60°, -45°)] with varying tilt angles relative to the bilayer normal were superimposed on drug bound $M2TM_{S31N}$ spectra (Fig. 4A-C). All spectra were collected at 720 MHz, pH 7.5, 303K. The molar ratio of lipid/protein was 30:1.

Figure 5. Superimposed 2D strip plots for $^{15}N/^{13}C$ (NCA) correlation spectra of $^{13}C,^{15}N$-$V_{27}A_{30}N_{31}G_{34}$ labeled $M2TM_{S31N}$ (residues 22-46) in DMPC lipid bilayers with (red) and without (blue) compound **6**. Spectra were collected at 600 MHz proton frequency, at pH 7.5, 10-kHz spinning rate and a calibrated temperature at sample of 263K.

Figure 6. Snapshots from the simulation of ligands bound to $M2TM_{WT}$. Waters within 10 Å from ligand are shown. **(a) 5** bound to $M2TM_{WT}$. Eight waters are shown between the ligand and H37

residues. Three hydrogen bonds between the secondary ammonium group of the ligand and three water molecules are shown (see Table S2). Hydrogen bonding together with van der Waals interactions of the adamantane core with V27 and A30 stabilize the ligand inside the pore with its ammonium group oriented towards the C-terminus. **(b) 6** bound to $M2TM_{WT}$. Eight waters are shown between the ligand and H37 residues. Two hydrogen bonds between the secondary ammonium group of the ligand and two water molecules are shown (see also Table S2). Hydrogen bonding together with van der Waals interactions of the adamantane core with V27 and A30 stabilize the ligand inside the pore with its ammonium group oriented towards the C-terminus.

Figure 7. Snapshots from the simulation of various ligands bound to $M2TM_{S31N}$. Waters within 10 Å from ligand are shown. Several waters are shown covering the region between the mouth the ligand and H37 residues. Few waters may be found between the ligands and the wall of the pore, suggesting a relatively free passage through the lumen. **(a) 1** bound to $M2TM_{S31N}$. Seven waters are shown between the ligand and H37 residues and six waters between N31 and the mouth of the pore. In the depicted shapshot one hydrogen bond between the ammonium group of the ligand and one water, and one hydrogen bond between the ligand and the carbonyl group of N31 amide side chain are shown (see also Table S3). No efficient van der Waals interactions can be formed for the adamantane core in the region close to A30 and the ligand can't be stabilized inside the pore. **(b) 5** bound to $M2TM_{S31N}$. Three waters are shown between the ligand and the region close to H37 residues and three waters between N31 and the mouth of the pore. One water is shown between the ligand and the wall of the pore. One hydrogen bond between the ammonium group of the ligand, and one water and two hydrogen bonds between the ligand and the carbonyl groups of two N31 amide side chain are shown (see also Table S3). Hydrogen bonding together with weak van der Waals interactions between the adamantane core and the cleft between A30 and G34 can weakly stabilize the ligand inside the pore with its ammonium group oriented towards the N-terminus. **(c) 6** bound to $M2TM_{S31N}$. Four waters are shown between the ligand and H37 residues and seven waters

between N31 and the mouth of the pore. Two hydrogen bonds between the ammonium group of the ligand and the carbonyl group of N31 amide side chain and one water are shown (see also Table S3). One water is shown between the ligand and the wall of the pore. Hydrogen bonding together with weak van der Waals interactions between the adamantane core and the cleft between A30 and G34 can weakly stabilize the ligand inside the pore with its ammonium group oriented towards the N-terminus. **(d) 10** bound to $M2TM_{S31N}$. Two waters are shown in the region between the ligand and H37 residues and six waters between N31 and the mouth of the pore. One water is shown between the ligand and the wall of the pore. Two hydrogen bonds between the ammonium group of the ligand and two waters are shown (see also Table S3). Hydrogen bonding together with weak van der Waals interactions between the adamantane core and the cleft between A30 and G34 can moderately stabilize the ligand inside the pore with its ammonium group oriented towards the N-terminus.

SCHEMES AND FIGURES

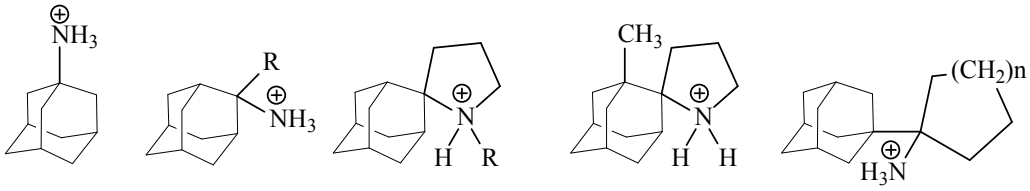

1

2: R=H
3: R=CH_3
4: R=C_2H_5
5: R=n-C_3H_7

6: R=H
7: R=CH_3

8

9: n=1
10: n=2

Scheme 1

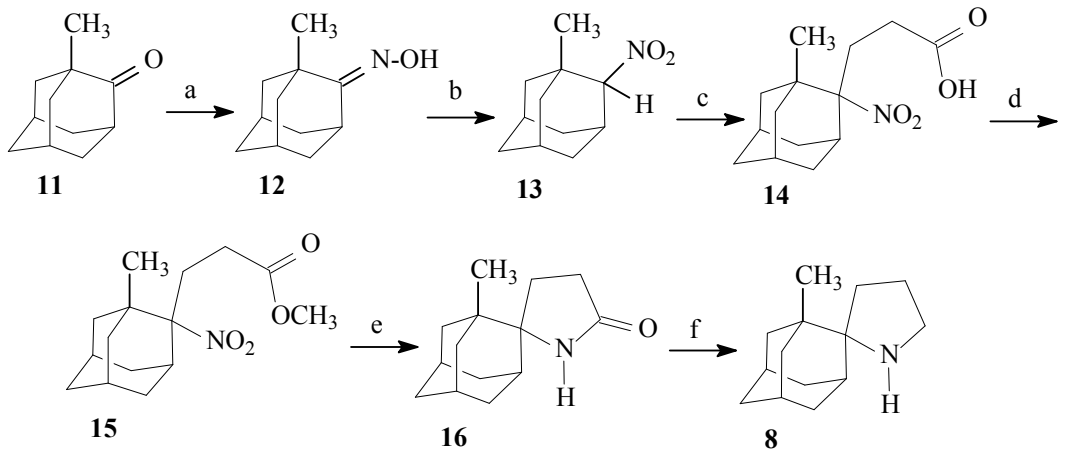

Reagents and conditions: (a) $H_2NOH{\cdot}HCl$, Na_2CO_3 90 ºC, 40 min (93%); (b) i. NBS, $NaHCO_3$, dioxane/water, 10 ºC, 40 min; ii. HNO_3, pentane, 0 ºC, 15 min; iii. $NaBH_4$, MeOH/H_2O; (c) i. $CH_2{=}CHCO_2Et$, Triton-B, t-BuOH, 70 ºC, 8 h ii. NaOH 1N, EtOH-H_2O 3:1, 70 ^{0}C, 8 h (89%); (d) MeOH/HCl(g), 60 ºC, 4 h, and then overnight at r.t. (79%); (e) H_2/Ni-Raney, EtOH, 50 psi, r.t., 24 h (84%); (f) $LiAlH_4$, THF, reflux, 48 h (60%).

Scheme 2

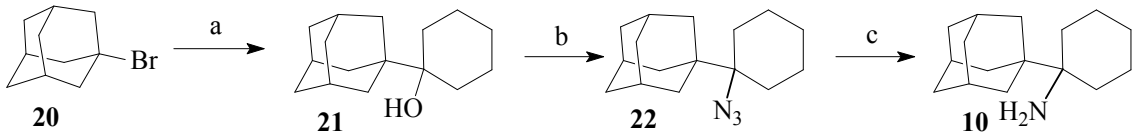

Reagents and conditions: (a) Li, dry THF, cyclohexanone, sonication, 0 ºC, 5h (70%); (b) NaN_3, TFA, CH_2Cl_2, 0 °C, 5h, then r.t. 24 h (35%). (c) $LiAlH_4$, dry ether, reflux, 5 h, then H_2O, NaOH 10% (65%).

Scheme 3

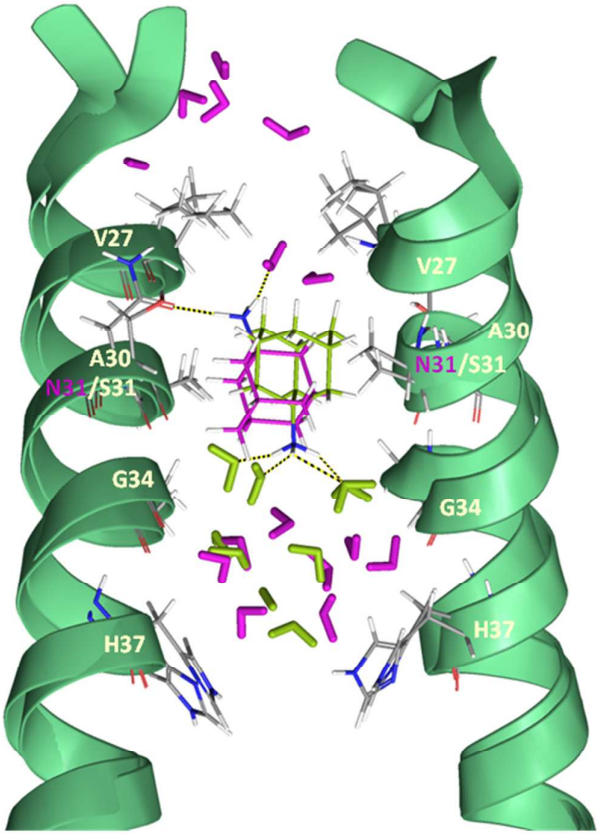

Figure 1

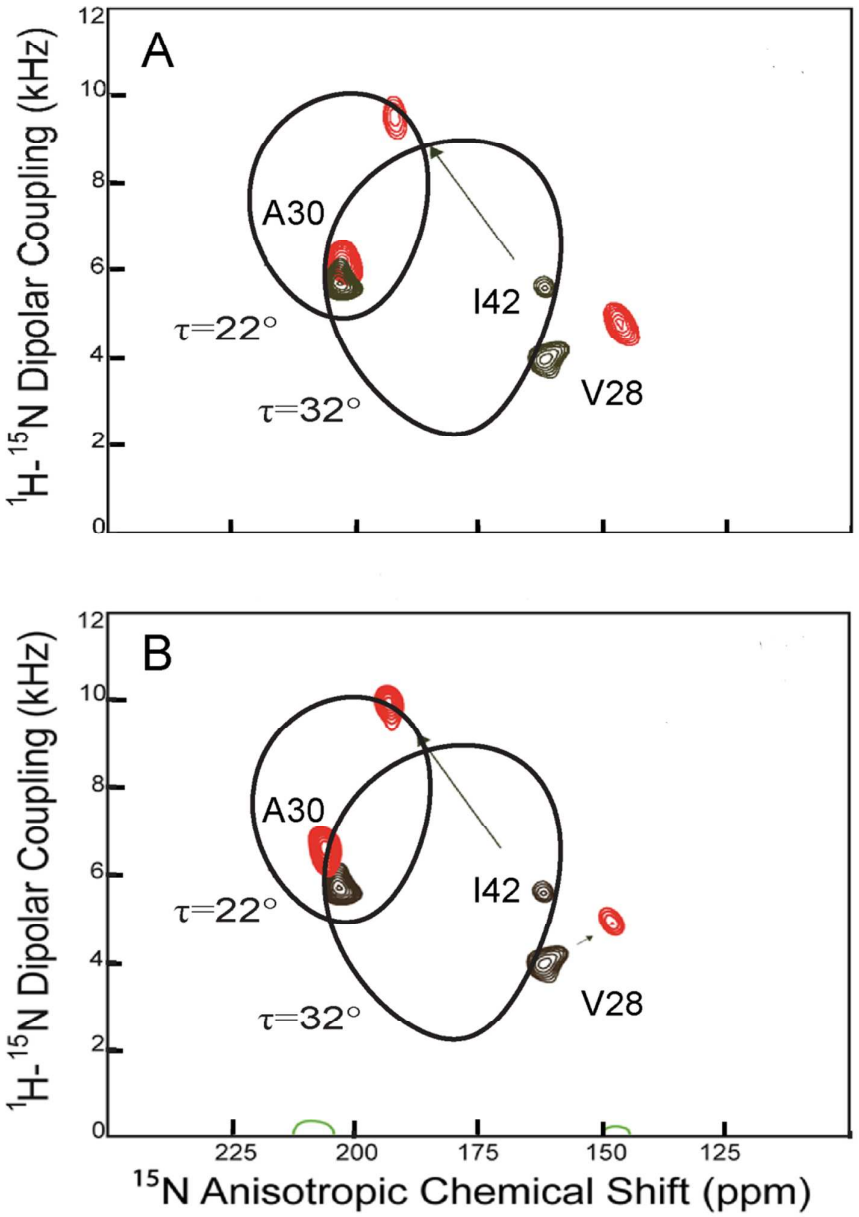
A
B
A30
I42
V28
τ=22°
τ=32°
^{1}H-^{15}N Dipolar Coupling (kHz)
^{15}N Anisotropic Chemical Shift (ppm)
0
2
4
6
8
10
12
225
200
175
150
125

Figure 2

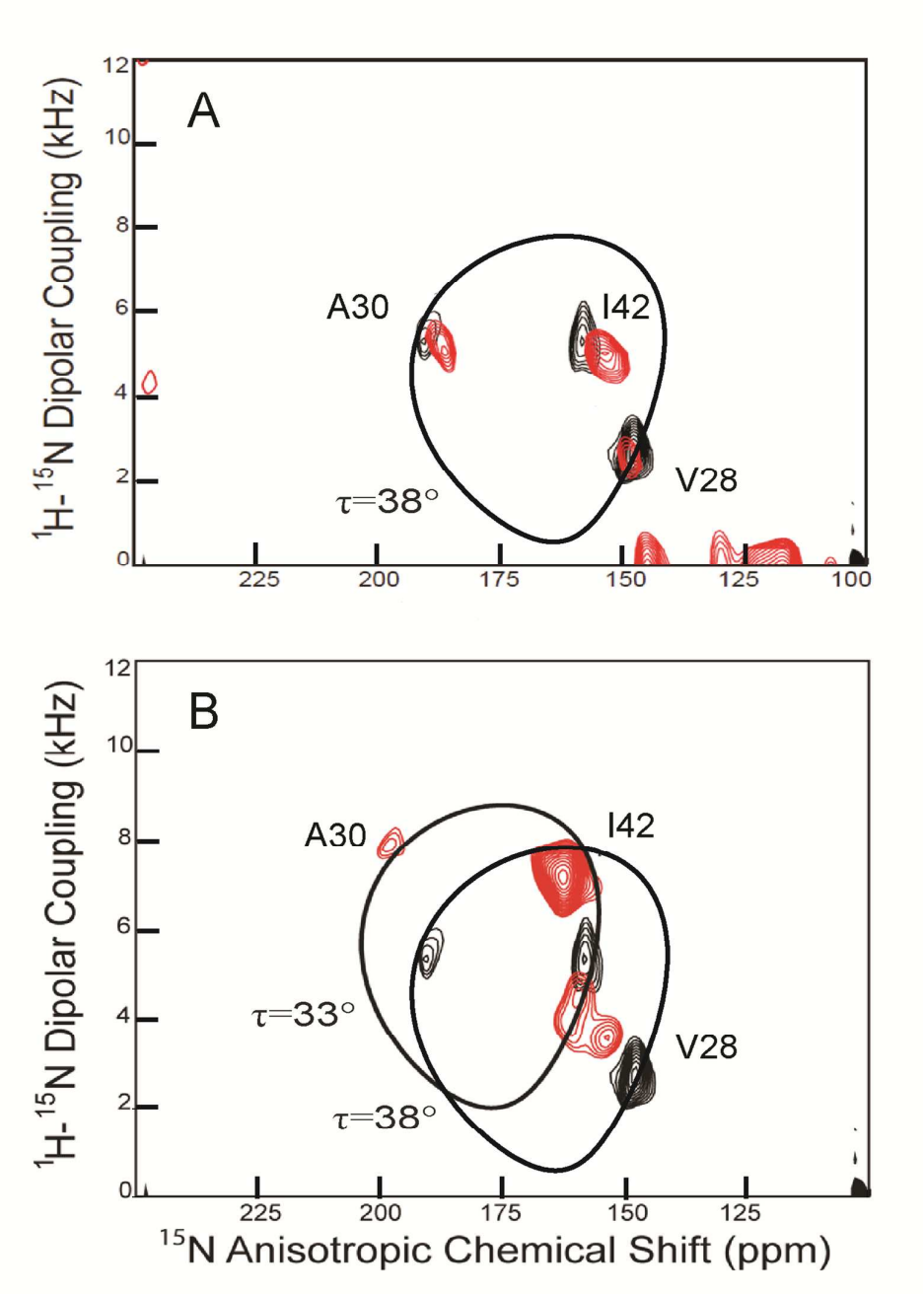
A
A30
I42
V28
τ=38°
B
A30
I42
V28
τ=33°
τ=38°
^{1}H-^{15}N Dipolar Coupling (kHz)
^{15}N Anisotropic Chemical Shift (ppm)
0
2
4
6
8
10
12
225
200
175
150
125
100

Figure 3

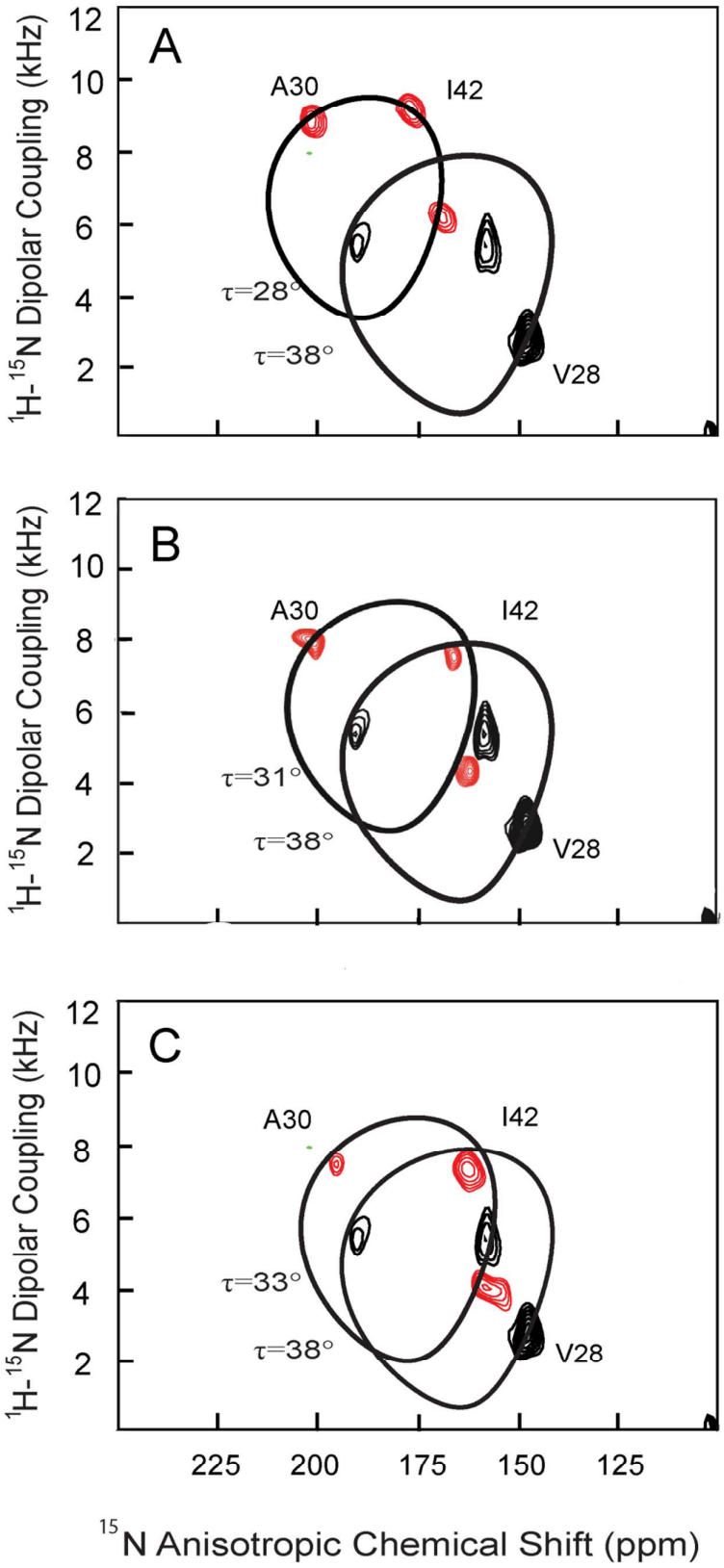
A
A30
I42
τ=28°
τ=38°
V28
B
A30
I42
τ=31°
τ=38°
V28
C
A30
I42
τ=33°
τ=38°
V28
12
10
8
6
4
2
225
200
175
150
125
1H-15N Dipolar Coupling (kHz)
15N Anisotropic Chemical Shift (ppm)

Figure 4

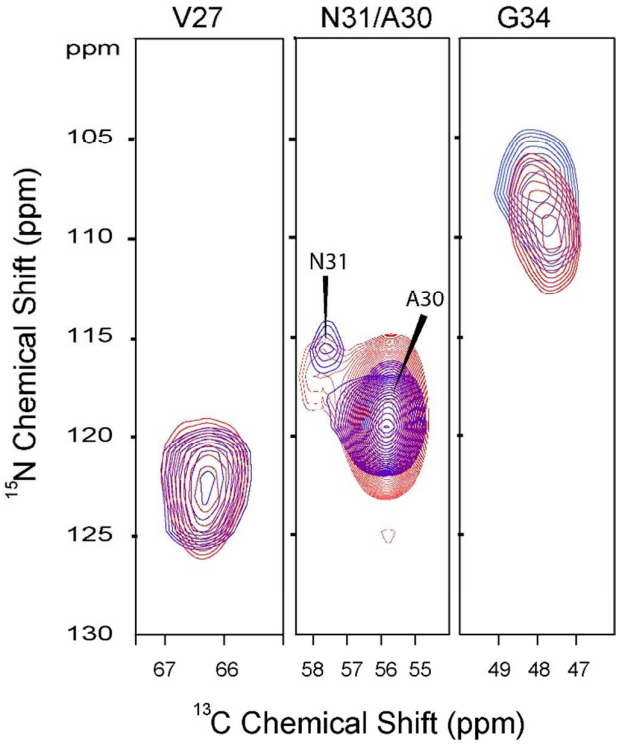
V27
N31/A30
G34
ppm
105
110
115
120
125
130
N31
A30
15N Chemical Shift (ppm)
67
66
58
57
56
55
49
48
47
13C Chemical Shift (ppm)

Figure 5

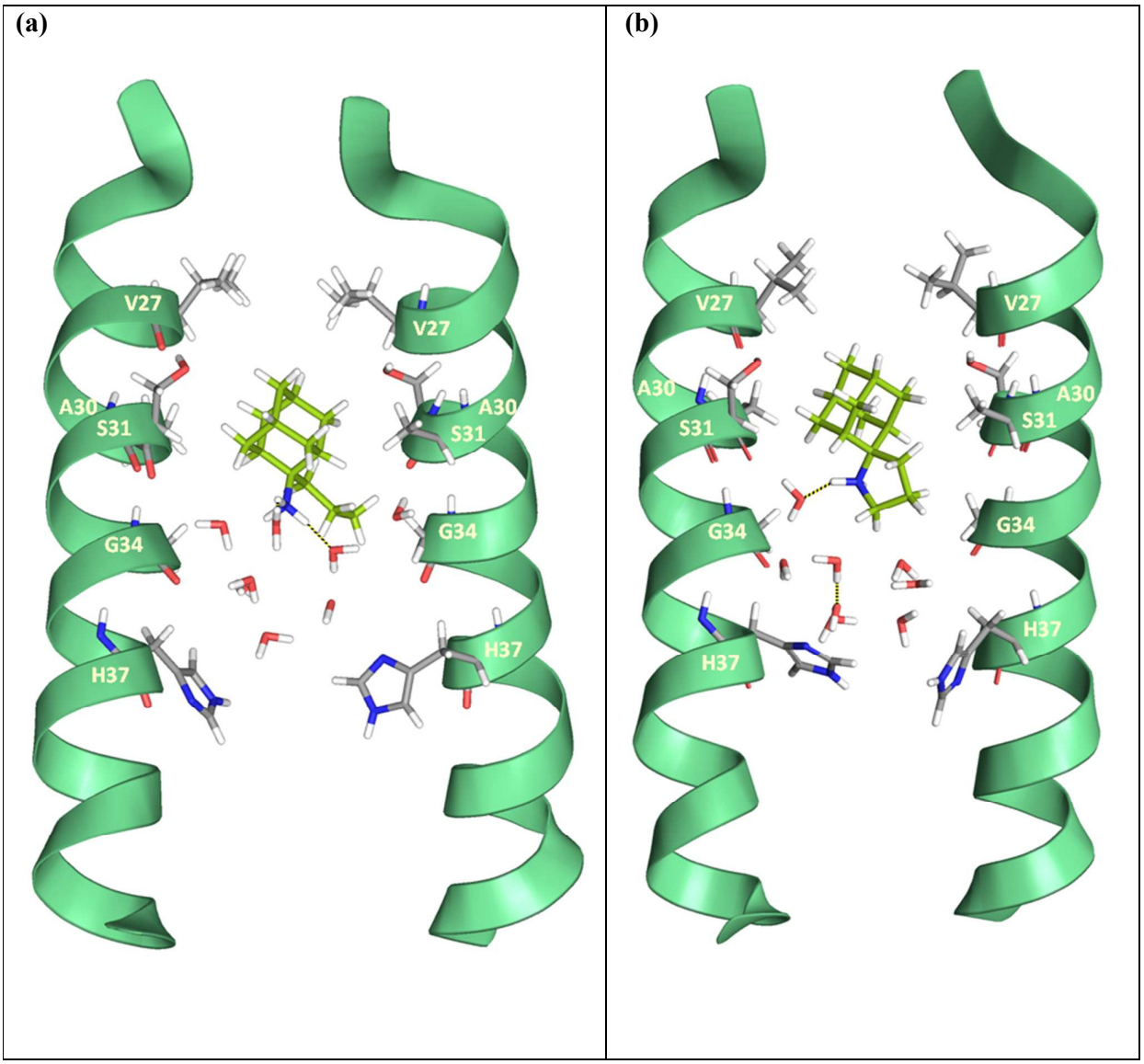
(a)
V27
V27
A30
S31
A30
S31
G34
G34
H37
H37
(b)
V27
V27
A30
S31
A30
S31
G34
G34
H37
H37

Figure 6

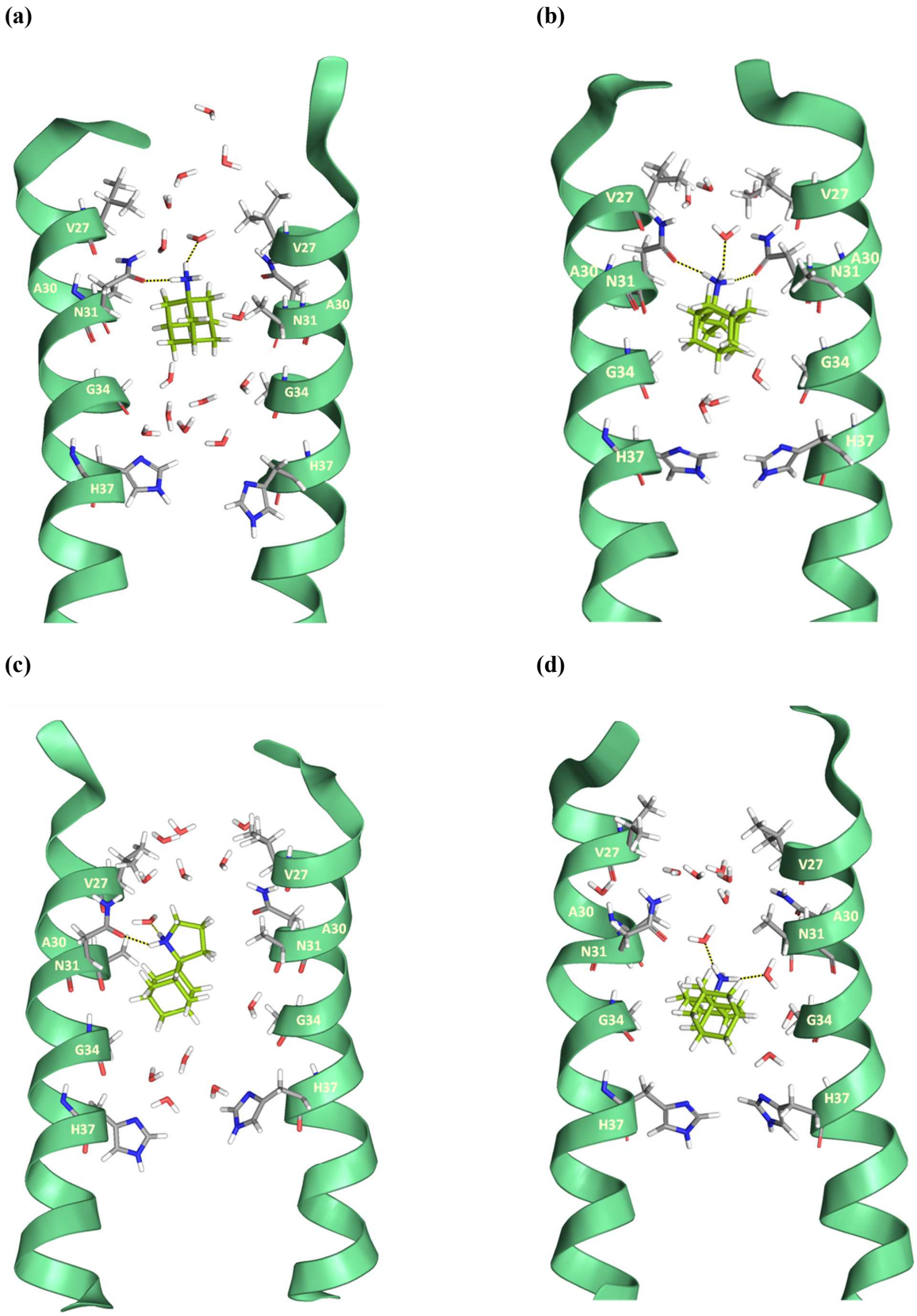
(a)
V27
V27
A30
N31
A30
N31
G34
G34
H37
H37
(b)
V27
V27
A30
N31
A30
N31
G34
G34
H37
H37
(c)
V27
V27
A30
N31
A30
N31
G34
G34
H37
H37
(d)
V27
V27
A30
N31
A30
N31
G34
G34
H37
H37

Figure 7

TABLES

Table 1. Binding constants, and other thermodynamic parameters derived from ITC measurements for influenza A $M2TM_{WT}$ and $M2TM_{S31N}$.

$M2TM_{WT}$				
Ligand [1]	**K_d** [2]	**ΔG** [3,4]	**ΔH** [3,5]	**$T\Delta S$** [3,6]
1 [7]	2.17 ± 0.52	-32.51 ± 0.59	-27.87 ± 2.09	4.64 ± 2.18
2 [7]	1.60 ± 0.34	-33.30 ± 0.54	-29.41 ± 1.76	3.89 ± 1.84
3 [7]	0.89 ± 0.19	-34.77 ± 0.54	-28.41 ± 1.09	6.32 ± 1.21
4 [7]	0.62 ± 0.14	-35.65 ± 0.54	-29.87 ± 0.88	5.77 ± 1.05
5 [7]	0.63 ± 0.17	-36.43 ± 0.69	-32.62 ± 1.29	3.90 ± 1.45
6 [7]	0.36 ± 0.22	-38.11 ± 1.84	-21.49 ± 1.76	16.61 ± 2.57
7 [7]	0.93 ± 0.36	-34.64 ± 0.96	-15.98 ± 1.17	18.66 ± 1.51
8 [7]	1.30 ± 0.43	-33.81 ± 0.84	-21.25 ± 1.30	12.55 ± 1.55
9	14.61 ± 4.62	-27.77 ± 0.79	- [8]	- [8]
10	> 10	- [8]	- [8]	- [8]

$M2TM_{S31N}$				
Ligand [1]	**K_d** [2]	**ΔG** [3,4]	**ΔH**	**$T\Delta S$**
1-4	- [9]	-	-	-
5	> 10	- [8]	- [8]	- [8]
6	17.5 ± 8.5	-27.95 ± 1.24	- [8]	- [8]
9	15.8 ± 5.95	-28.22 ± 0.96	- [8]	- [8]
10	9.90 ± 4.99	-29.41 ± 1.29	- [8]	- [8]

[1] See Scheme 1.

[2] Binding constant K_d in μM calculated from measured K_a in M^{-1} by $K_d = 1/K_a \times 10^{-6}$ and error in K_d in μM determined by $K_{d,\,error} = (K_{a,\,error}/K_a^2) \times 10^{-6}$.

[3] In kJ mol^{-1}.

[4] Free energy of binding computed from K_d by $\Delta G = -RT \ln(K_d^{ref}/K_d)$ with $K_d^{ref} = 1$ M and $T = 300$ K and error in ΔG determined according to

$$\Delta G_{error} = \sqrt{\left(\frac{R\,T\,K_{d,\,error}}{K_d}\right)^2}$$

with $T = 300$ K.

[5] Enthalpy of binding and error in the enthalpy of binding calculated from measured binding enthalpy and measured error by $\Delta H = \Delta H_{measured}\,(\,T\,/\,T_{measured}\,)$ with $T = 300$ K and the temperature at which the ITC measurements were performed $T_{measured} = 293.15$ K.

[6] Entropy of binding calculated by $\Delta S = (-\Delta G + \Delta H)/T$ and error in ΔS computed by the equation

$$\Delta S_{error} = \sqrt{\Delta G_{error}^{\;2} + \Delta H_{error}^{\;2}}$$

[7] Measured in ref. 24.

[8] Values could not be determined reliably due to the limitations of the methods in the area of very weak binding.

[9] No detectable binding.

Table 2. Mean helical tilt values relative to the bilayer normal from MD simulations of **1**, **5** in complex with $M2TM_{WT}$ in DMPC bilayer.

Ligand [1]	MD simulations [2]	ssNMR Experiment [3]	2KQT [4a,5b]
	N-terminus /C-terminus	N-terminus /C-terminus	N-terminus /C-terminus
1	31º ± 4.6º / 18º ± 4.9º	32 ± 2° / 22° ± 2°	30° / 19°
5	31º ± 5.1º / 19º ± 5.0º	32 ± 2° / 22° ± 2°	

[1] See Scheme 1.

[2] Calculated using Gromacs tools.

[3] This study.

Table 3. Mean helical tilt values relative to the bilayer normal from MD simulations of **5-8** in complex with $M2TM_{S31N}$ in DMPC bilayer.

Ligand [1]	MD simulations [2]	Experiment [3,4]
1	34 º ± 4º	38º ± 1º
5	31º ± 6º	33º ± 1º
6	28º ± 5º	28º ± 1º
7	33º ± 4º	31º ± 1º
8	31º ± 4º	33º ± 1º

[1] See Scheme 1.

[2] Calculated using Gromacs tools.

[3] This study.

[4] Helical tilt is uniform.

Table 4. Block of full-length M2-dependent currents by select compounds in transfected HEK cells.[1]

Compound	A/California/07/2009 (H1N1) M2: N31		A/California/09/2009 (H1N1) M2: S31	
	% Block after 3m	% Block after 30m	% Block after 3m	IC_{50}
1 [2]	14 ± 2 (100 μM; 26)	(N/A)	75 ± 9 (10 μM; 4)	2 ± 3 (3)
2 [2]	13 ± 3 (100 μM; 2)	16 (100 μM; 1)	95 ± 8 (10 μM; 2)	2 ± 1 μM (2)
5 [2]	0 ± 5 (100 μM; 2)	9 ± 10 (100 μM, 3)	63 ± 5 (10 μM; 2)	7 ± 2 μM (2)
6	4 ± 3 (100 μM; 2)	5 ± 4 (100 μM, 2)	66 ± 6 (10 μM; 3)	5 ± 2 μM (3)
9	4 ± 4 (100 μM; 2)	4 ± 10 (100 μM; 4)	46 ± 2 (10 μM; 2)	10 ± 2 μM (2)

[1] For each compound, percent block of pH-dependent M2 current at listed concentrations (+/- s.e.m.) and/or IC_{50} (μM) is shown. Parenthesis show number of replicates.

[2] Data were also reported in Ref. 10a.

Table 5. Antiviral activity of compounds **1–10** against influenza virus A/WSN/33 (H1N1) variants in Madin-Darby canine kidney cells.

Compound	IC_{50} (μM) [1]		CC_{50} (μM) [2]
	A/WSN/33-M2-N31S	A/WSN/33-M2-N31	
1	0.27±0.16	N.A.[3]	>100 [4]
2	0.42±0.46	N.A.	70.50±25.31
3	0.33±0.10	N.A.	25.63±7.65
4	0.34±0.26	N.A.	>100
5	0.34±0.10	N.A.	>100
6	0.34±0.08	N.A.	>100
7	0.90±0.29	N.A.	>100
8	6.12±2.59	N.A.	>100
9	4.34±2.94	N.A.	>100
10	N.A.	N.A.	>100
Oseltamivir	0.02±0.01	0.02±0.01	Not determined

[1] Mean and standard deviations of the 50% inhibitory concentration (IC_{50}) of at least three independent measures.

[2] Mean and standard deviations of the 50% cytotoxic concentration (CC_{50}) of at least three independent measures.

[3] N.A., not active, maximum concentration tested: 100 μM.

[4] Exact value published in ref. 46.

TOC Graphic

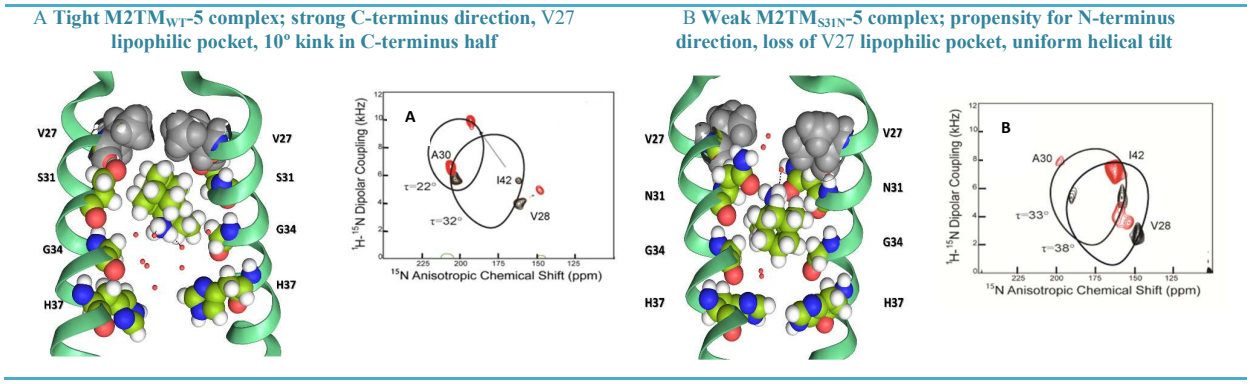
A Tight M2TM$_{WT}$-5 complex; strong C-terminus direction, V27 lipophilic pocket, 10º kink in C-terminus half
B Weak M2TM$_{S31N}$-5 complex; propensity for N-terminus direction, loss of V27 lipophilic pocket, uniform helical tilt
V27
S31
G34
H37
N31
A
B
A30
I42
V28
τ=22°
τ=32°
τ=33°
τ=38°
^{1}H-^{15}N Dipolar Coupling (kHz)
^{15}N Anisotropic Chemical Shift (ppm)